Bioorganic Chemistry 112 (2021) 104965

Contents lists available at ScienceDirect

Bioorganic Chemistry

journal homepage: www.elsevier.com/locate/bioorg

Design and discovery of new antiproliferative 1,2,4-triazin-3(2*H*)-ones as tubulin polymerization inhibitors targeting colchicine binding site

Ibrahim H. Eissa [a,*], Mohammed A. Dahab [a,b,*], Mohamed K. Ibrahim [a], Nawaf A. Alsaif [c], A. Z. Alanazi [d], Sally I. Eissa [e,f], Ahmed B.M. Mehany [g], André M. Beauchemin [b]

[a] Pharmaceutical Medicinal Chemistry & Drug Design Department, Faculty of Pharmacy (Boys), Al-Azhar University, Cairo, 11884, Egypt
[b] Centre for Catalysis Research and Innovation, Department of Chemistry and Biomolecular Sciences, University of Ottawa, Ontario K1N6N5, Canada
[c] Department of Pharmaceutical Chemistry, College of Pharmacy, King Saud University, Riyadh, Saudi Arabia
[d] Department of pharmacology and toxicology, College of Pharmacy, King Saud University, Riyadh, Saudi Arabia
[e] Department of Pharmaceutical Chemistry, Faculty of Pharmacy (Girls), Al-Azhar University, Cairo, Egypt
[f] Department of Pharmaceutical Sciences, College of Pharmacy, AlMaarefa University, Dariyah, Riyadh, 13713, Saudi Arabia
[g] Department of Zoology, Faculty of Science (Boys), Al-Azhar University, Cairo, 11884, Egypt

ARTICLE INFO

Keywords:
Anti-cancer
Colchicine analogues
Tubulin polymerization
Docking
1,2,4-Triazin-3(2*H*)-ones

ABSTRACT

Thirty-five new colchicine binding site inhibitors have been designed and synthesized based on the 1,2,4-triazin-3(2*H*)-one nucleus. Such molecules were synthesized through a cascade reaction between readily accessible α-amino ketones and phenyl carbazate as a masked *N*-isocyanate precursor. The synthesized derivatives are cisoid restricted combretastatin A4 analogues containing 1,2,4-triazin-3(2*H*)-one in place of the olefinic bond, and they have the same essential pharmacophoric features of colchicine binding site inhibitors. The synthesized compounds were evaluated *in vitro* for their antiproliferative activities against a panel of three human cancer cell lines (MCF-7, HepG-2, and HCT-116), using colchicine as a positive control. Among them, two compounds **5i** and **6i** demonstrated a significant antiproliferative effect against all cell lines with IC_{50} ranging from 8.2 – 18.2 μM. Further investigation was carried out for the most active cytotoxic agents as tubulin polymerization inhibitors. Compounds **5i** and **6i** effectively inhibited microtubule assembly with IC_{50} values ranging from 3.9 to 7.8 μM. Tubulin polymerization assay results were found to be comparable with the cytotoxicity results. The cell cycle analysis revealed significant G2/M cell cycle arrest of the analogue **5i** in HepG-2 cells. The most active compounds **4i, 4j, 5 g, 5i** and **6i** did not induce significant cell death in normal human lung cells Wl-38, suggesting their selectivity against cancer cells. Also, These compounds upregulated the level of active caspase-3 and boosted the levels of the pro-apoptotic protein Bax by five to seven folds in comparison to the control. Moreover, apoptosis analyses were conducted for compound **5i** to evaluate its apoptotic potential. Finally, *in silico* studies were conducted to reveal the probable interaction with the colchicine binding site. ADME prediction study of the designed compounds showed that they are not only with promising tubulin polymerization inhibitory activity but also with favorable pharmacokinetic and drug-likeness properties.

1. Introduction

Microtubule dynamics is an important target for developing anti-cancer agents [1]. The tubulin heterodimer contains three distinct drug binding sites: the paclitaxel (taxanes alkaloid), vinblastine (vinca alkaloid), and colchicine binding sites (CBS) [2]. Colchicine **I** (Fig. 1) is the oldest antimitotic agent known and it has been the first line therapy for the treatment of acute gouty arthritis and familial Mediterranean fever (FMF) [3-5]. Additionally, due to the anti-fibrotic and anti-inflammatory activities, the therapeutic use of colchicine has extended beyond gouty arthritis, to atherosclerosis, osteoarthritis, and pericarditis [6-10]. However, due to the efficiency and high inhibition observed for tubulin polymerization, hundreds of analogues have been prepared recently to maintain colchicine's antimitotic abilities but reduce toxicity to the biological organism [11-16]. Colchicine binding site inhibitors (CBSIs) exert their biological effects by inhibiting tubulin assembly and

* Corresponding authors at: Pharmaceutical Medicinal Chemistry & Drug Design Department, Faculty of Pharmacy (Boys), Al-Azhar University, Cairo, 11884, Egypt (I.H. Eissa and M.A. Dahab).
E-mail addresses: Ibrahimeissa@azhar.edu.eg (I.H. Eissa), mohammeddahab@azhar.edu.eg (M.A. Dahab).

https://doi.org/10.1016/j.bioorg.2021.104965
Received 4 September 2020; Received in revised form 7 April 2021; Accepted 3 May 2021
Available online 5 May 2021

suppressing microtubule formation [17]. Colchicine itself binds to tubulin very tightly, but neither colchicine nor compounds that bind to the colchicine binding site on tubulin have yet found significant use in cancer treatment [18]. Combretastatin A-4 (CA-4) **II** (Fig. 1) has been identified as a promising anticancer agent that selectively targets tumor vasculature [19-22]. The activity of CA-4 is hampered by the poor metabolic stability and the weak water solubility due to the isomerization of the active z-olefinic conformation into the corresponding inactive *trans*-analogs [23,24]. To overcome this problem, several analogues have been extensively investigated to retain the potency and efficacy of CA-4, but with different pharmacokinetic profile [25-32]. Many cyclic structures have been investigated to replace the olefinic bridge, including three, five and six-membered rings, e.g., compounds **III** and **IV** [33-41] (Fig. 1). Even fused carbocyclic compounds have also been advanced as molecules that modify the ethylene bridge of CA-4, e.g., compounds **V** [42-44] (Fig. 1). In the last few decades, 1,2,4-triazine derivatives have expanded significantly, especially as a vital heterocyclic class of antitumor agents. Some of the 1,2,4-triazine derivatives that displayed potential anticancer activity have undergone clinical trials [45-49]. Recently, 5,6-diaryl-1,2,4-triazines were prepared and evaluated for their cytotoxic activities. Some of them showed potent cytotoxic activity e.g., compounds **VI** (IC_{50} = 16.10 μM), [50] (Fig. 1). Interestingly, in this approach the prepared compounds lack some of the essential pharmacophoric features which are important for the activity. The two phenyl rings have to be substituted with one or more methoxy groups. These methoxy groups play a dual role for the binding with the colchicine binding site, since they act as hydrogen bond acceptors and hydrophobic centers as well (Fig. 3). For this purpose and in continuation to our previous efforts of design and synthesis of new anticancer agents [51-59], we developed a mild cascade reaction to access some new 1,2,4-triazin-3(2*H*)-one derivatives. The synthesized compounds have the essential pharmacophoric features of CBSIs with different electronic properties. In silico studies were performed to investigate their binding pattern with the prospective target (colchicine binding site of tubulin protein).

1.1. Rational drug design

The colchicine binding site is positioned at the interface between the α and β subunits of the tubulin protein, having a funnel shape (Fig. 2). The 1st side of the cavity is surrounded by Val181α, Asn101α, Ala180α, Thr179α, Asn349β, Asn350β, Lys352β, and Thr314β residues. The 2nd side of the cavity is bordered by Val238β, Tyr202β, Thr239β, Leu242β, Leu252β, Cys241β, Ile378β, Leu248β, Val318β, and Leu255β residues. The 3rd side is surrounded by Asp251β, Ala250β, Met259β, Lys254β, Asn258β, Ala316β, Thr353β, Ala354β, Ala317β and residues.

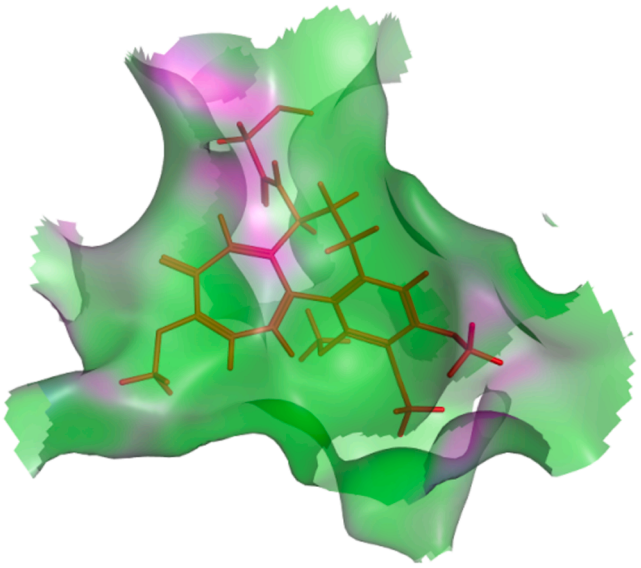

Fig. 2. The colchicine binding site having a funnel shape (isolated pocket of tubulin heterodimers obtained from Protein Data Bank (PDB ID: 1sa0) using MOE 2014 software).

According to many reports [60-63], CBSIs have seven main pharmacophoric features. These include three hydrogen bond acceptors (A1, A2, and A3), one hydrogen bond donor (D1), two hydrophobic centers (H1 and H2), and one planar group (R1) (Fig. 3**A**). The seven pharmacophoric points are allocated in two planes separated by an acute angle of 45°. The 1st plane comprises the features of A1, D1, H1, and R1. The 2nd plane includes the features of A2, A3, and H2 **(**Fig. 3**B).** Colchicine and combretastatin A-4 as representative examples of CBSIs are consisted of three parts: "A" ring, "B" ring (linker), and "C" ring. Many reports [64-66] revealed that modification of the "B" ring could affect the cytotoxic activity of the CBSIs (Fig. 3**C & 3D**).

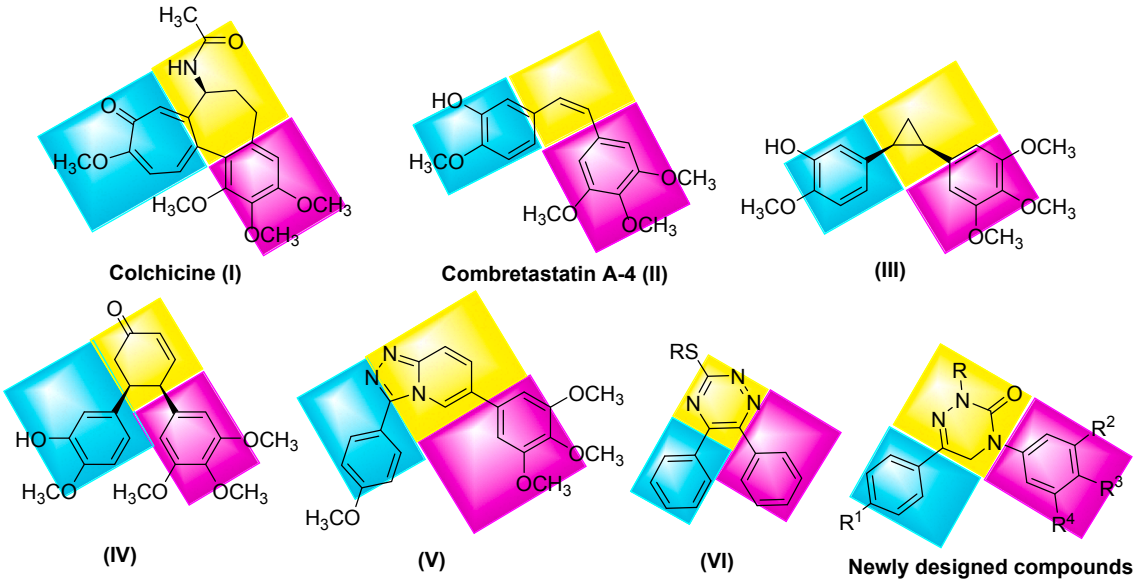

Fig. 1. Chemical structures of some reported CBSIs in which the olefinic bridge of CA-4 is replaced by cyclic structures [40-42,50], and the general structure of our target compounds.

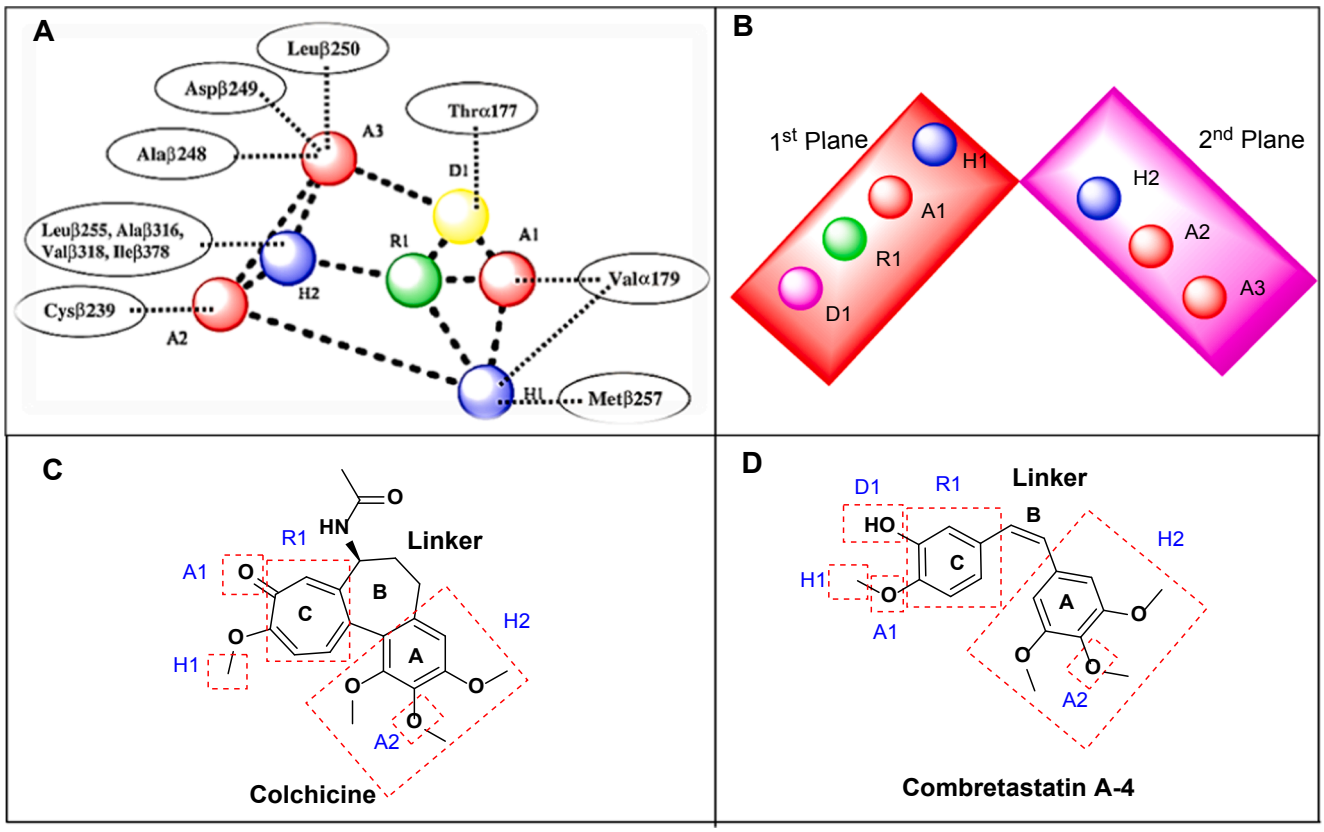

Fig. 3. **A**) The essential pharmacophoric features of CBSIs: hydrogen bond acceptors (A1, A2 & A3), hydrogen bond donor (D1), hydrophobic centers (H1 & H2), and planar group (R1) (based on Ref. [60,61]). **B**) The pharmacophoric model with two planes: the 1st plane (red) (A1, D1, H1 and R1); the 2nd Plane (pink) (A2, A3, and H2) (based on Ref. [52,60]). **C&D**) Pharmacophoric points of colchicine and combretastatin A-4 as CBSIs. (For interpretation of the references to colour in this figure legend, the reader is referred to the web version of this article.)

In this study, we replaced the olefinic bridge with 1,2,4-triazin-3(2*H*)-one ring to mimic the relative orientation induced by the Z-alkene configuration of CA-4. Such strategy produced many CA-4 analogs having the same essential pharmacophoric features of the reported tubulin inhibitors. The second aim was focused on modification of the "A" ring, "C" ring, and linker region to study the structure–activity relationship of the synthesized compounds as new cytotoxic agents targeting CBS. Accordingly, the "A" ring could be phenyl, *para*-methoxyphenyl, 3,5-di methoxyphenyl, or 3,4,5-trimethoxyphenyl group. The "C" ring could be phenyl or *para*-methoxyphenyl group. The linker region was designed to be 1,2,4-triazin-3(2*H*)-one ring. The choice of this moiety was based on some considerations. i) The ring itself comprises HBA and HBD points which act as essential pharmacophoric features. ii) The non-planar configuration of the ring is consistent with the non-planar configuration of the middle ring of colchicine.

In a separate approach, we focused on the modification of the 1,2,4-triazin-3(2*H*)-one "B" ring of the designed compounds. Such modification was achieved by chemical substitutions of esters, acids, or amides side chains at the NH group. These substituents could also have the essential HBA and HBD features and possess the same spatial orientation of acetamide side chain of colchicine. All modification pathways and molecular design rationale are illustrated and summarized in Fig. 4.

2. Results and discussion

2.1. Chemistry

In continuation for our previous work of synthesis of heterocyclic structures using *N*-isocyanates as reactive intermediates [67-77], new 1,2,4-triazin-3(2*H*)-one derivatives have been synthesized. A mild cascade synthesis of 1,2,4-triazin-3(2*H*)-ones was reported from readily accessible α-amino ketones [78,79] and phenyl carbazate as a masked *N*-isocyanate precursor, under acidic condition [67]. Phenyl carbazate were synthesized by the improved method developed by Beauchemin group [80] through dropwise addition of hydrazine (1.0 M) in THF over diphenyl carbonate in petroleum ether as solvent (around 90% yield). Also, α-amino ketones (**2a-e**) were prepared by simple mixing of two equivalent of the amine with one equivalent of the corresponding α-haloketone in MeCN and stir overnight at room temperature. Then, acid catalyzed condensation of α-amino ketones (**2a-e**) with phenyl carbazate, followed by intramolecular cyclization on the *N*-isocyanate intermediate to give the target compounds **3a-e** (Scheme 1).

In this work, we were interested in a complementary approach involving, i) alkylation of –NH group of the triazine moiety to form a panel of esters with one or two carbon bridge (**4a-j**). ii) Hydrolysis of the synthesized esters to form the corresponding acids (**5a-j**). iii) Alkylation of –NH group of the triazine moiety to form a panel of amides with one carbon or two carbon bridge (**6a-j**) (Scheme 2).

Ester derivatives of 1,2,4-triazin-3(2*H*)-one (**4a-j**) were synthesized via the reaction of 1,2,4-triazin-3(2*H*)-ones (**3a-e**) with ethyl bromoacetate or ethyl 3-bromopropionate in DMF in presence of NaH. The role of NaH was to ease the replacement of relatively stable acidic 1,2,4-triazin-3(2*H*)-ones proton and to prevent the accumulation of acid byproduct which can cause the decomposition of the formed ester. In case of ethyl bromoacetate the reaction was complete in about 30 min, while in case of ethyl 3-brompropionate it needed to be heated at reflux in DMF for around 4 h. The ester derivatives (**4a-j**) were confirmed by ^{1}H NMR spectra, which showed the disappearance of the singlet signal of –NH proton of triazine ring and the appearance of a new two signals (for acetate) or three signals (for propionate) for the ester methylene proton

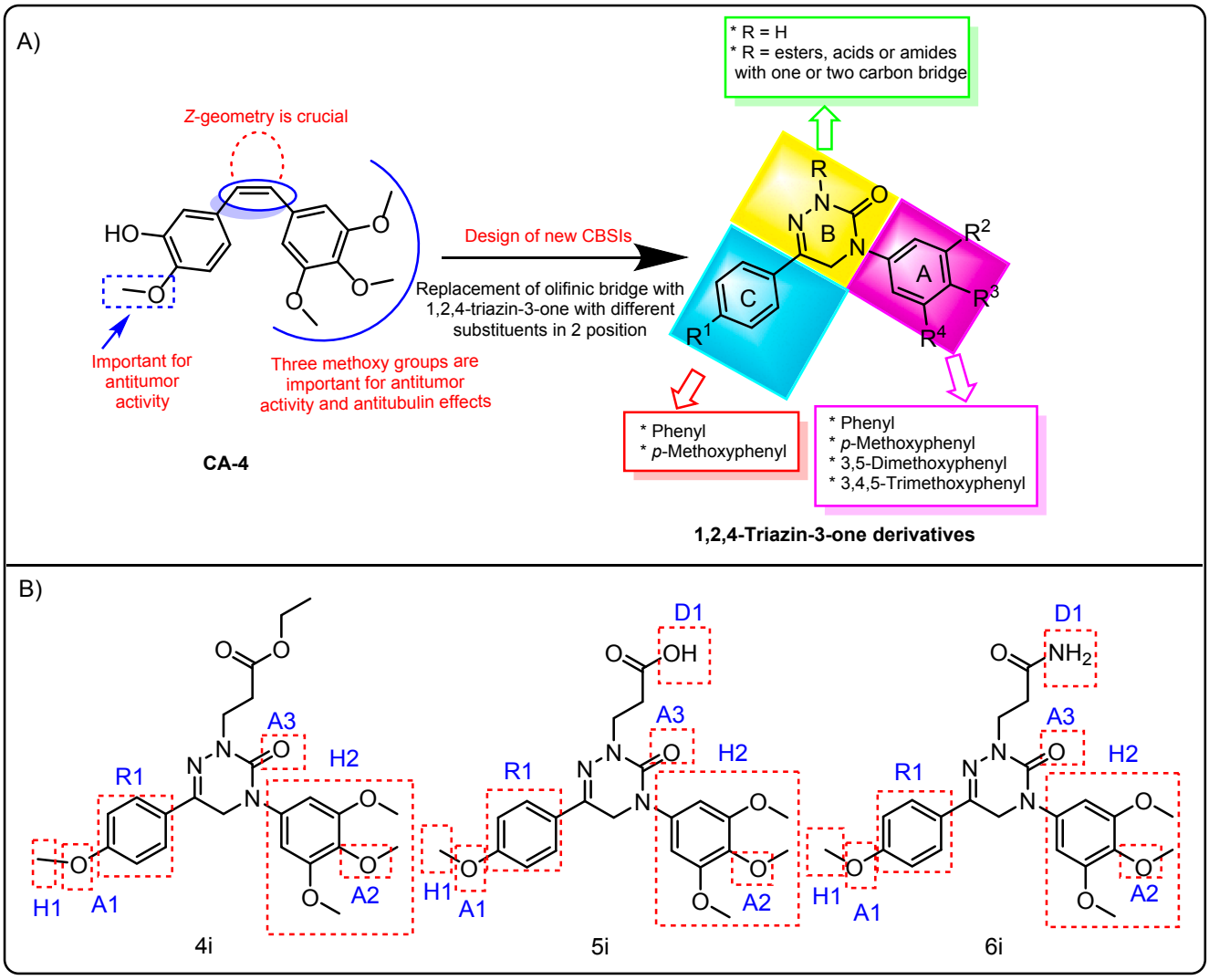

Fig. 4. A) Rational of molecular design of the new proposed CBSIs based on CA-4. **B)** Some new 1,2,4-triazin-3(2*H*)-ones having the essential pharmacophoric features of the reported CBSIs.

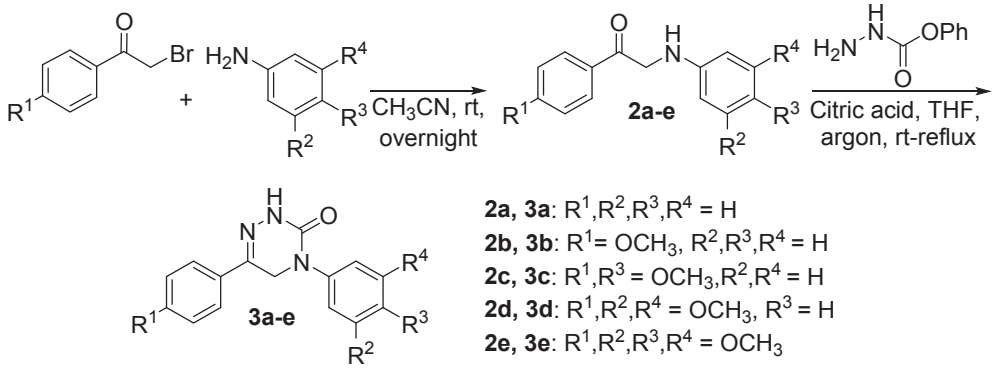

Scheme 1. Syntheses of 1,2,4-triazin-3(2*H*)-ones using *N*-isocyanate cascade reaction.

in the range of δ 2.80 – 4.20 ppm. This methylene proton was also detected in both of ^{13}C NMR and DEPT 135 NMR spectra resonating in the range of δ 30.0 – 50.0 ppm. Also, ^{1}H NMR spectra showed the presence of triplet signal at a range of δ 1.20–1.30 ppm corresponding to the methyl group of the ester.

Acid derivatives (**5a-j**) were prepared by hydrolysis of the corresponding esters (**4a-j**) via refluxing with NaOH, in CH_3OH as solvent. The acid derivatives **(5a-j)** were confirmed by ^{1}H NMR spectra, which showed the disappearance of the methyl and one of the methylene protons of the ester, with appearance of a new broad singlet signal in a range of δ 10.50 – 11.00 ppm corresponding to the carboxylic group of the acid. The disappearance of the ester methylene protons was also confirmed by ^{13}C NMR and DEPT 135 NMR spectra.

Amide derivatives of 1,2,4-triazin-3(2*H*)-one (**6a-j**) were synthesized

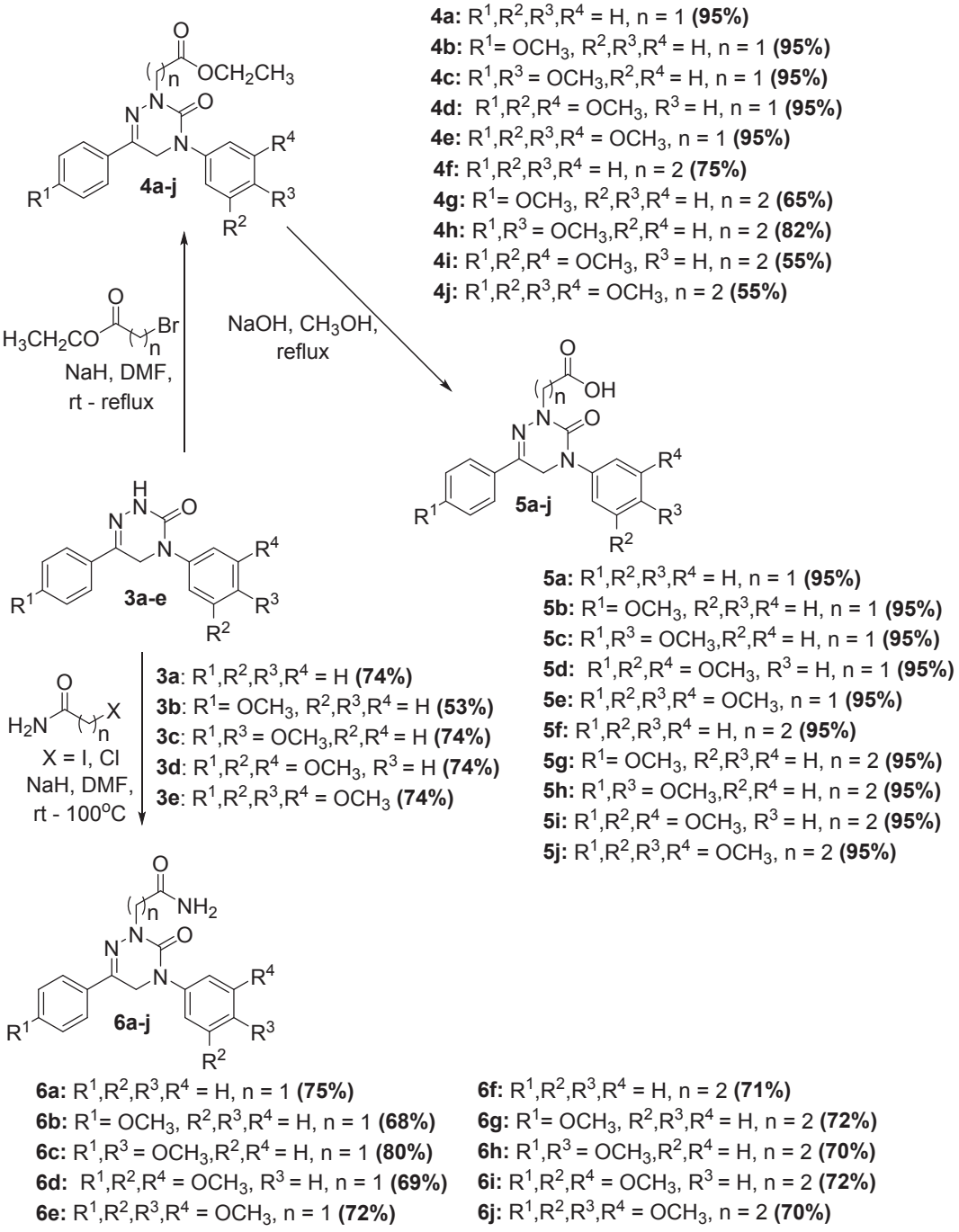

Scheme 2. Synthesis of the target compounds **4a-j, 5a-j** and **6a-j** (Isolated yields in parentheses).

via the reaction of 1,2,4-triazin-3(2*H*)-ones (**3a-e**) with iodoacetamide or 3-chloropropanamide in DMF in presence of NaH. In case of iodoacetamide the reaction was completed in about one hour, while in case of 3-chloropropanamide it needed heating at 100 ^{O}C for around 4 h. The amide derivatives (**6a-j**) were confirmed by ^{1}H NMR spectra, which showed the disappearance of the singlet signal of –NH proton of triazine ring and the appearance of a new singlet signal (for acetamide) or two triplet signals (for propionamide) for the methylene protons in a range of δ 2.80 – 4.20 ppm. This methylene proton was also confirmed by both ^{13}C NMR and DEPT 135 NMR spectra resonating in a range of δ 35.0 – 50.0 ppm. Also, ^{1}H NMR spectra showed the presence of two separated singlet signals at a range of δ 5.70–6.60 ppm corresponding to the amino group protons.

2.2. Biological evaluation

2.2.1. In vitro anti-proliferative activity

The synthesized compounds were tested for their *in vitro* cytotoxic activities using standard MTT method [81,82] against a group of human cancer cell lines namely, breast cancer (MCF-7), hepatocellular carcinoma (HepG-2) and colorectal carcinoma (HCT-116). Colchicine was used as a positive control. The results of cytotoxicity test were reported as growth inhibitory concentration (IC_{50}) values and summarized in Table 1.

The tested compounds exhibited different degrees of anti-proliferative activities against the three tested cell lines. In general, compounds **3b, 4i, 4j, 5 g, 5i, 6f** and **6i** showed superior anti-proliferative activities against the three cell lines with IC_{50} values

Table 1
In vitro anti-proliferative activities of the tested compounds and tubulin polymerization inhibition.

Comp.	*In vitro* cytotoxicity IC_{50} (μM)[a]			Tubulin polymerization Inhibition IC_{50} (μM)[a]
	MCF-7	HepG-2	HCT116	
3a	133.9 ± 2.1	167.7 ± 2.3	186.9 ± 2.5	NT[b]
3b	35.9 ± 1.3	**19.9 ± 0.9**	**30.6 ± 1.2**	285.1 ± 1.73
3c	62.1 ± 1.8	70.1 ± 1.7	83.0 ± 1.9	NT[b]
3d	133.7 ± 2.4	151.0 ± 2.7	211.7 ± 2.9	NT[b]
3e	77.1 ± 1.7	67.7 ± 1.5	86.0 ± 2.1	55.8 ± 1.22
4a	108.3 ± 2.3	97.0 ± 2.4	160.8 ± 2.8	NT[b]
4b	307.1 ± 5.7	298.4 ± 4.4	344.4 ± 6.1	NT[b]
4c	213.4 ± 3.5	176.6 ± 3.8	218.9 ± 3.9	NT[b]
4d	169.1 ± 2.3	154.8 ± 3.6	204.7 ± 2.7	NT[b]
4e	103.5 ± 3.4	120.1 ± 3.5	145.5 ± 4.2	NT[b]
4f	101.4 ± 2.2	85.8 ± 2.4	121.4 ± 3.4	33.9 ± 0.95
4 g	156.7 ± 3.9	201.2 ± 4.2	196.0 ± 4.6	NT[b]
4 h	119.6 ± 3.4	111.8 ± 3.2	156.9 ± 2.8	NT[b]
4i	**20.5 ± 1.7**	**14.4 ± 1.1**	**22.4 ± 1.5**	**17.7 ± 0.75**
4j	**23.1 ± 1.5**	**18.5 ± 1.2**	**25.1 ± 1.4**	**22.3 ± 0.92**
5a	77.3 ± 2.3	85.8 ± 1.9	112.0 ± 2.5	NT[b]
5b	341.6 ± 6.3	328.3 ± 5.7	369.3 ± 7.4	NT[b]
5c	56.1 ± 2.9	95.7 ± 2.5	107.3 ± 3.5	NT[b]
5d	63.7 ± 3.8	49.6 ± 2.8	70.4 ± 3.6	NT[b]
5e	139.2 ± 2.7	158.7 ± 2.9	180.2 ± 2.3	NT[b]
5f	162.8 ± 1.4	180.8 ± 1.4	226.6 ± 1.3	NT[b]
5 g	**42.2 ± 3.2**	**23.2 ± 3.1**	**33.1 ± 3.8**	**28.0 ± 0.87**
5 h	77.6 ± 3.6	91.9 ± 3.6	123.4 ± 4.5	NT[b]
5i	**10.9 ± 0.84**	**8.2 ± 0.63**	**15.7 ± 1.2**	**3.9 ± 0.06**
5j	86.2 ± 2.8	100.7 ± 2.8	139.7 ± 3.3	NT[b]
6a	89.6 ± 2.1	76.6 ± 2.3	107.8 ± 2.6	NT[b]
6b	346.7 ± 6.2	268.5 ± 5.9	358.6 ± 6.5	NT[b]
6c	255.2 ± 3.9	216.3 ± 2.5	311.1 ± 4.1	NT[b]
6d	192.0 ± 2.2	184.7 ± 1.5	229.1 ± 2.3	105.0 ± 1.33
6e	185.0 ± 3.8	177.8 ± 3.8	203.5 ± 4.9	NT[b]
6f	**29.2 ± 3.4**	35.7 ± 4.1	**29.2 ± 4.6**	37.9 ± 0.98
6 g	122.7 ± 1.2	131.8 ± 0.71	184.9 ± 1.3	NT[b]
6 h	144.2 ± 2.8	164.1 ± 2.7	196.9 ± 4.6	NT[b]
6i	**16.3 ± 0.71**	**11.2 ± 0.42**	**18.2 ± 0.73**	**7.8 ± 0.15**
6j	82.6 ± 2.7	89.1 ± 3.1	119.2 ± 4.1	NT[b]
Colchicine	34.3 ± 1.16	27.3 ± 0.97	31.1 ± 1.1	28.6 ± 0.95
CA-4	0.67 ± 0.13[c]	16.04 ± 0.50[c]	9.00 ± 0.85[c]	2.03 ± 0.41[d]

In bold: the most potent compounds
[a] IC_{50} values are the mean ± S.D. (standard deviations) of three separate experiments.
[b] NT: stands for (Not Tested)
[c] These IC_{50} values were retrieved from reference[85]
[d] This IC_{50} value were retrieved from reference[86]

ranging from 8.2 to 42.2 μM. The cytotoxic activities of compounds **4i, 4j, 5i,** and **6i** were higher than that of the reference drug, colchicine (IC_{50} = 34.3, 27.3 and 31.1 μM against MCF-7, HepG-2 and HCT-116, respectively).

2.2.2. Tubulin polymerization assay

To investigate whether the cytotoxic activity of the synthesized compounds was related to an interaction with the tubulin system, tubulin polymerization assay was performed for the most cytotoxic compounds **3b, 3e, 4f, 4i, 4j, 5 g, 5i, 6d, 6f** and **6i**. The inhibition of microtubule polymerization was evaluated turbidimetrically using a fluorescent plate reader [83,84]. Colchicine was used as a positive control (Table 1).

The results revealed that compounds **4i, 4j, 5i** and **6i** were the most potent tubulin polymerization inhibitors with an IC_{50} values ranging from 3.9 to 22.3 μM. These compounds had activities higher than that of colchicine (IC_{50} = 28.6 μM). We can conclude that the cytotoxic activity of the synthesized compounds may be due to an interaction with tubulin and an interference with microtubule assembly.

2.2.3. Cell cycle analysis

Antimitotic drugs induced cell cycle arrest at G2/M phase in various cancer cell lines [87]. In order to investigate the impact of compound **3e** and **5i** on growth inhibition of cancer cells, their activities on the cell cycle distribution and apoptosis induction were assessed using HepG-2 cell lines according to the method described by Wand *et al* [88,89]. In the present work, HepG-2 cell line was treated with compounds **3e** and **5i** at concentrations of 67.7 and 8.2 μM, respectively for 24 h.

The results revealed that incubation compounds **3e**, **5i** and colchicine with HepG-2 cells produced marked increase of HepG-2 cells at G2/M phase from 20.6% to 38.4%, 24.7%, and 47.3%, respectively. On the other hand, such percentages decreased at S and G0-G1 phases. Such results indicate that the synthesized compounds caused cell arrest at G2/M phase. Moreover, the tested compounds as well as colchicine produced an increase of the cell population at Pre-G1, indicating that compound **3e** and **5i** caused apoptotic effect at pre-G1 phase (Table 2 and Fig. 5**)**.

2.2.4. Annexin V-FITC apoptosis assay

Apoptosis is a programmed cell death which plays a key role in the maintenance of tissue homeostasis and cell survival [90]. Thus, inducing apoptosis in cancer cells has emerged as an attractive strategy in cancer therapy. To further confirm apoptotic effect of compounds **3e,** and **5i** in HepG-2 cells, Annexin V and PI double staining assay was performed [91]. In this test, HepG-2 cells were incubated with compound **3e** and **5i** at concentrations of 67.7 and 8.2 μM respectively for 24 h. The results in Table 3, Fig. 6. revealed that compound **3e** induced total apoptotic effect equal 13.7% which was nine times more than the control cells (1.5%). Also, it induced early apoptosis by 6.2% and enhanced late apoptosis by 5.3% when compared with the untreated control HepG-2 cells (0.5% and

Table 2
Effect of compound **3e** and **5i** on cell cycle progression.

Sample	Cell cycle distribution (%)			
	%G0-G1	%S	%G2-M	%Pre-G1
3e / HepG-2	36.3	25.3	38.4	13.7
5i / HepG-2	45.1	30.3	24.7	13.5
Control / HepG-2	51.6	27.8	20.6	1.5
Colchicine / HepG-2	29.7	22.9	47.3	22.6

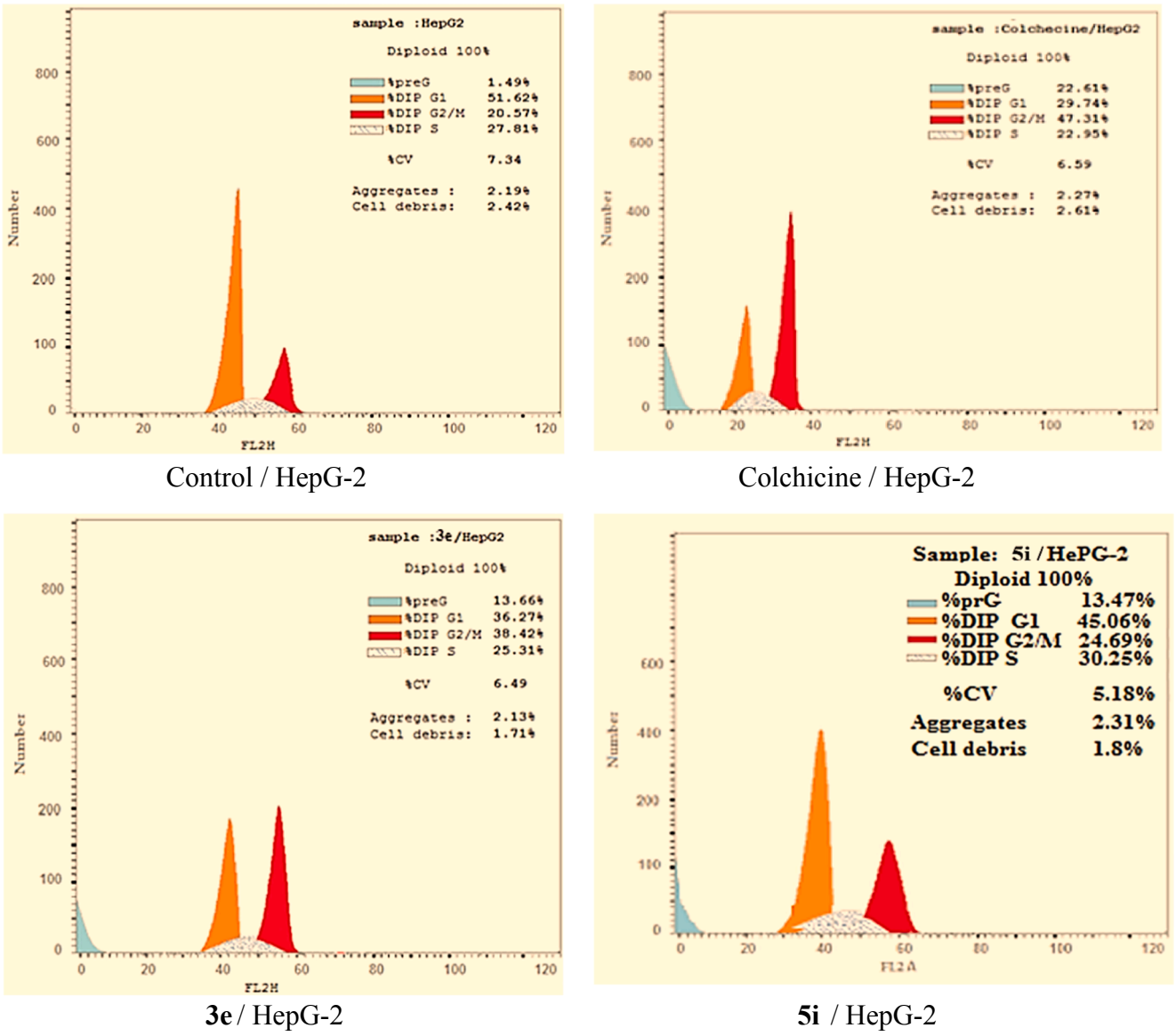

Fig. 5. HepG-2 cells distribution upon treatment with compound **3e, 5i** and colchicine.

Table 3
Apoptosis and necrosis percent induced by compound **3e, 5i,** and colchicine.

Sample	Apoptosis			Necrosis
	Total	Early	Late	
3e / HepG-2	13.7	6.2	5.3	2.2
5i / HepG-2	13.5	4.1	7.1	2.3
Control / HepG-2	1.5	0.5	0.2	0.8
Colchicine / HepG-2	22.6	7.4	12.9	2.3

0.2%, respectively). For compound **5i**, it induced total apoptotic effect equal 13.5% which was nine times more than the control cells (1.5%). Furthermore, it induced early apoptosis by 4.1% and enhanced late apoptosis by 7.1% when compared with the untreated control HepG-2 (0.5% and 0.2%, respectively).

2.2.5. *In vitro cytotoxicity against human normal cell*

One of the main problems of cancer chemotherapy is the unwanted damage to normal cells caused by the high toxicities of anticancer drugs. The most promising compounds **4i, 4j, 5 g, 5i** and **6i** were further investigated *in vitro* against WI-38 cell line (normal human lung fibroblasts) using MTT assay and their IC_{50} were determined.

The results revealed that IC_{50} doses of all the tested compounds against WI-38 cells were very high in comparison to their IC_{50} doses against the cancer cell lines by six to eleven-fold (Table 4). Such results indicate that compounds **4i, 4j, 5 g, 5i** and **6i** have a significant effect in rapidly proliferating cells but not in normal cells.

2.2.6. *Caspase-3 determination*

Caspases are the primary drivers of apoptotic cell death [92]. Caspase-3 is the most well-characterized effector caspase which is the executioner caspase activated by upstream initiator caspases [93]. Thus, the investigation of this protein expression level is indicative of apoptosis induction. To find out whether the most promising compounds **4i, 4j, 5 g, 5i** and **6i** induced caspase-3 dependent apoptosis, HepG-2 cells were treated with such compounds at concentrations of 14.4, 18.5, 23.2, 8.2, and 11.2 μM, respectively for 48 h and the levels of caspase-3 were assessed. The results revealed that the tested compounds upregulated the caspase-3 levels from three to six folds as compared to the control. These findings prove apoptosis induction potential of the tested compounds (Table 5).

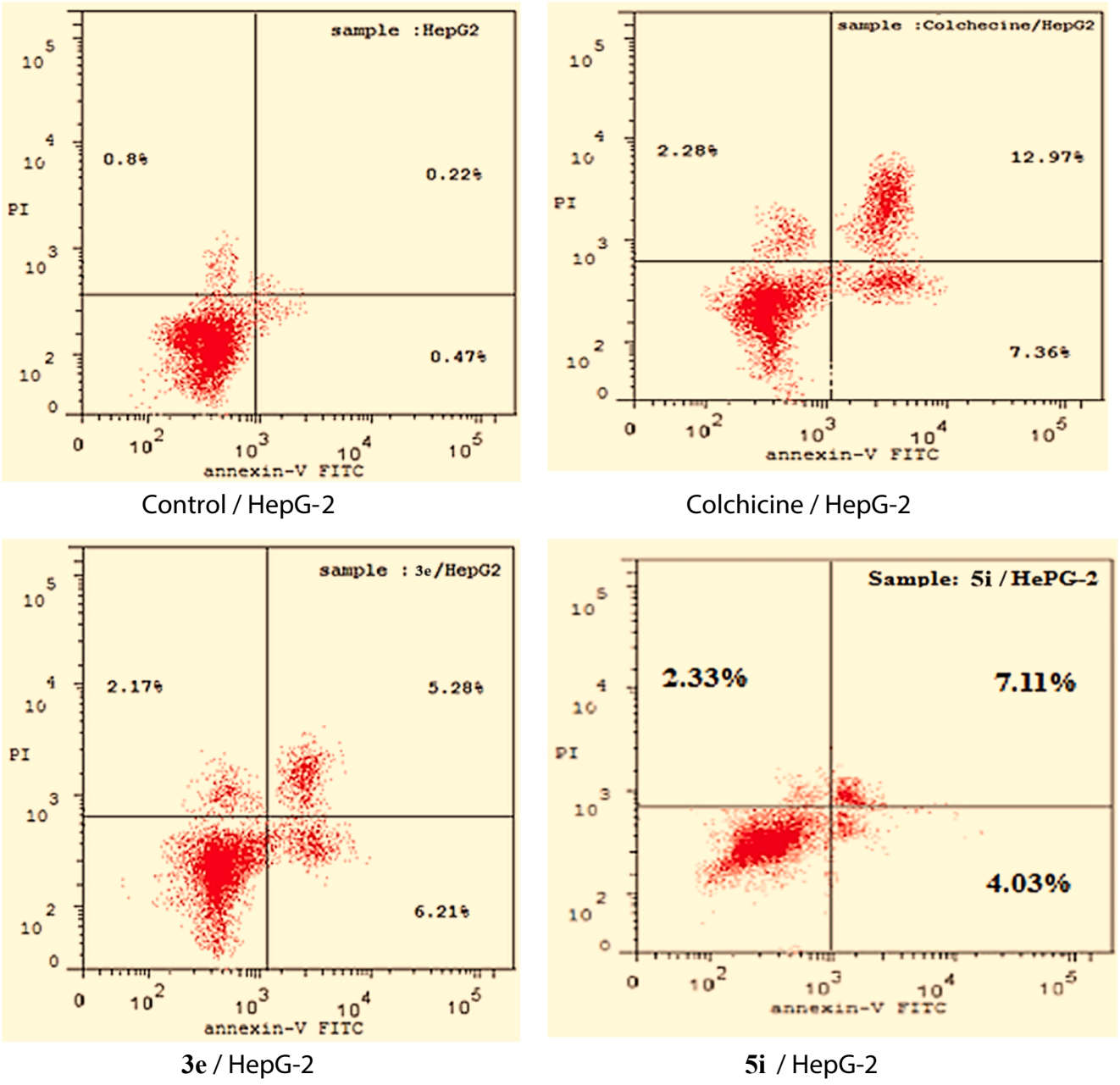

Fig. 6. Apoptosis and necrosis percent induced by compound **3e, 5i,** and colchicine.

Table 4
in vitro cytotoxicity of compounds **4i, 4j, 5 g, 5i** and **6i** on normal WI-38 cells.

Comp.	WI-38 IC_{50} (μM)[a]
4i	139.2 ± 5.3
4j	179.6 ± 4.1
5 g	187.3 ± 5.4
5i	127.1 ± 3.6
6i	170.6 ± 3.5

[a] IC_{50} values are the mean ± S.D. (standard deviations) of three separate experiments.

2.2.7. *Bax determination*

The apoptotic regulation depends mainly on a family of proteins responsible for synchronizing the mitochondrial apoptotic pathway [94], e.g. Bax which induces apoptosis (pro-apoptotic). In this context, HepG-2 cells were treated with compounds **4i, 4j, 5 g, 5i** and **6i** at concentrations of 14.4, 18.5, 23.2, 8.2, and 11.2 μM, respectively for 48 h and their effects on the levels of Bax were determined as illustrated in Table 5. The results revealed that these compounds boosted the levels of the pro-apoptotic protein Bax by five to seven folds as compared to the

Table 5
Effect of the compounds **4i, 4j, 5 g, 5i,** and **6i** on caspase-3 and Bax expression levels.

Comp.	**Caspase-3 (Pg/mL)**[a]	**Bax (Pg/mL)**[a]
4i	282.4 ± 5.7	311.6 ± 1.3
4j	215.6 ± 4.6	285.8 ± 2.4
5 g	226.1 ± 4.2	308.6 ± 2.3
5i	321.3 ± 6.8	387.2 ± 2.9
6i	247.8 ± 4.3	350.4 ± 1.7
Control / HepG-2	60.3 ± 2.5	56.1 ± 1.1

[a] The values (in picogram per mL) given are means ± SD of three experiments.

control cells, emphasizing that these compounds shifted the cells towards undergoing apoptosis. This data revealed that these compounds induced cell death by apoptosis in human lung cancer cells.

2.3. In silico studies

2.3.1. Flexible alignment

3D- flexible alignment of representative compound **4i** with colchicine is presented in Fig. 7. In the figure is possible to observe that, in general, the structure of compound **4i** has a good overlap with the reference molecule (colchicine).

2.3.2. Docking studies

Discovery Studio 4.0 software was used for the docking simulations against 3D structure of tubulin heterodimers obtained from Protein Data Bank (PDB ID: 1sa0). DAMA-colchicine, the native ligand, and colchicine were used as reference ligands (See Table 6).

DAMA-colchicine gave a binding energy value of −42.84 kcal/mol. The "A" ring (trimethoxy phenyl) occupied the first pocket of the colchicine binding site forming four hydrophobic interactions with Leu255, Ala250, Ala316, and Cys241. The "B" ring with its side chain (2-mercaptoacetamide moiety) occupied the second cavity of the colchicine binding site forming a hydrogen bond with Leu254. Also, it formed two hydrophobic interactions with Leu248 and Ala250. Furthermore, the "C" ring (methoxytropone moiety) occupied the third pocket of the receptor forming two hydrogen bonds with Ser187 (Fig. 8).

Compound **4i** showed a binding mode like that of the co-crystallized ligand (DAMA-colchicine), with affinity value of −64.54 kcal/mol. The trimethoxy phenyl moiety ("A" ring) occupied the first cavity of the colchicine binding site forming one hydrophobic interaction with Lys254. Additionally, the 4,5-dihydro-1,2,4-triazin-3(2*H*)-one moiety ("B" ring) and its ethyl propionate side chain occupied the second cavity of the colchicine binding site forming two hydrogen bonds with Ala250 and Cys241. In addition, it formed two hydrophobic interactions with Leu242 and Leu255. The p-methoxyphenyl moiety ("C" ring) occupied the third cavity of the colchicine binding site forming two hydrophobic interactions with Ala316 and Lys352 (Fig. 9).

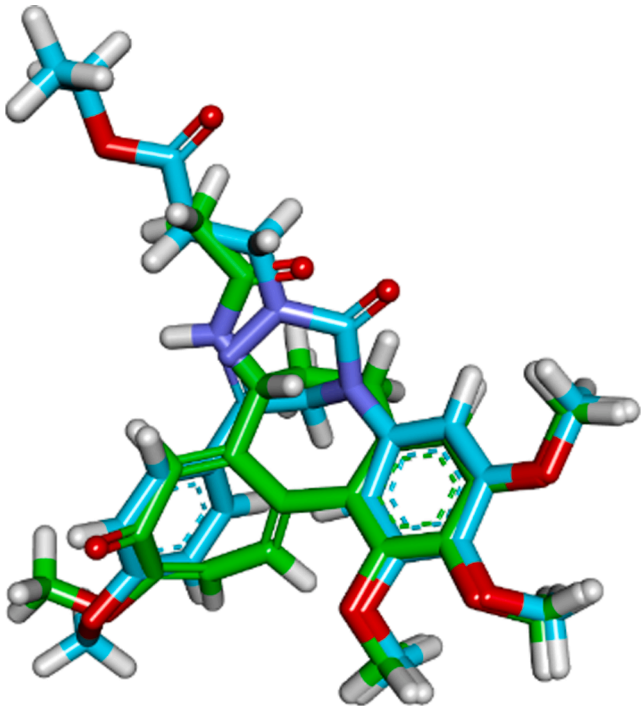

Fig. 7. Flexible alignment of compounds **4i** (carbon atoms in turquoise) with the colchicine (carbon atoms in green). (For interpretation of the references to colour in this figure legend, the reader is referred to the web version of this article.)

Table 6
The docking scores of the synthesized compounds, colchicine, and co-crystallized ligand (DAMA-colchicine) against tubulin.

Comp.	Binding free energy (kcal/mol)	Comp.	Binding free energy (kcal/mol)
3a	−33.77	**5e**	−62.63
3b	−39.46	**5f**	−46.13
3c	−43.71	**5 g**	−54.47
3d	−47.95	**5 h**	−59.18
3e	−53.51	**5i**	−60.05
4a	−48.21	**5j**	−63.04
4b	−49.56	**6a**	−43.09
4c	−52.38	**6b**	−46.17
4d	−59.41	**6c**	−51.58
4e	−65.85	**6d**	−58.96
4f	−50.41	**6e**	−59.69
4 g	−53.46	**6f**	−44.61
4 h	−58.84	**6 g**	−47.96
4i	−64.54	**6 h**	−49.81
4j	−60.95	**6i**	−60.02
5a	−45.66	**6j**	−60.48
5b	−50.77	**DAMA-colchicine**	−42.84
5c	−52.43	**Colchicine**	−59.16
5d	−58.84		

The binding modes of compounds **5i, 5j, 6i and 6j** are depicted in **Supplementary Data**.

2.3.3. In silico ADMET analysis

ADMET studies were carried out for the most cytotoxic members **4i, 4j, 5 g, 5i,** and **6i**. Colchicine was used as a reference drug. Discovery studio 4.0 was used to predict ADMET descriptors for all compounds. The predicted descriptors are listed in Table 7.

The results revealed that the tested compounds have low or very low BBB penetration levels. Accordingly, such compounds were expected to be safe to CNS. All the tested compounds showed good to optimal range levels of ADMET aqueous solubility. Also, all compounds were appeared to have good intestinal absorption levels [95]. All examined members were predicted as non-inhibitors of CYP2D6. Consequently, liver dysfunction side effect is not expected upon administration of these compounds [96]. All compounds were expected to bind plasma protein over than>90% (Fig. 10.).

(The predicted toxicity studies, Physico-chemical properties and Lipinski rule of five are depicted in Supplementary Data)

2.4. Structure-Activity relationship (SAR)

Based on the aforementioned biological data, many structure–activity relationships could be deduced. With respect to substitution on "A" ring, the decreased IC_{50} values of compounds **4i, 5i, 6i**, **4j, 5j,** and **6j** than the corresponding members **4 h, 5 h,** and **6 h**, indicated that substitution of "A" ring with 3,5-di methoxy or 3,4,5-trimethoxy is more advantagous. For "B" ring, comparing the activity of compounds **3e** (unsubstituted), **4i** (ester substituted), **5i** (acid substituted), and **6i** (amide substituted), indicated that substitution of 1,2,4-triazine ring at 2-position with ester, acid, or amide is tolerated. Interestingly, ester (**4f-j**), acid (**5f-j**), and amide (**6f-j**) derivatives with two carbon bridge exhibited higher activities than the corresponding members with one carbon bridge (**4a-e**), (**5a-e),** and (**6a-e**), hinting that elongation of the linker enhances the antiproliferative activity. Furthermore, the decreased IC_{50} values of compounds **3b, 4i, 5i,** and **6i** than the corresponding members **3a, 4a, 5a,** and **6a**, suggesting that the substitution in "C" ring is favorable (See Fig. 11).

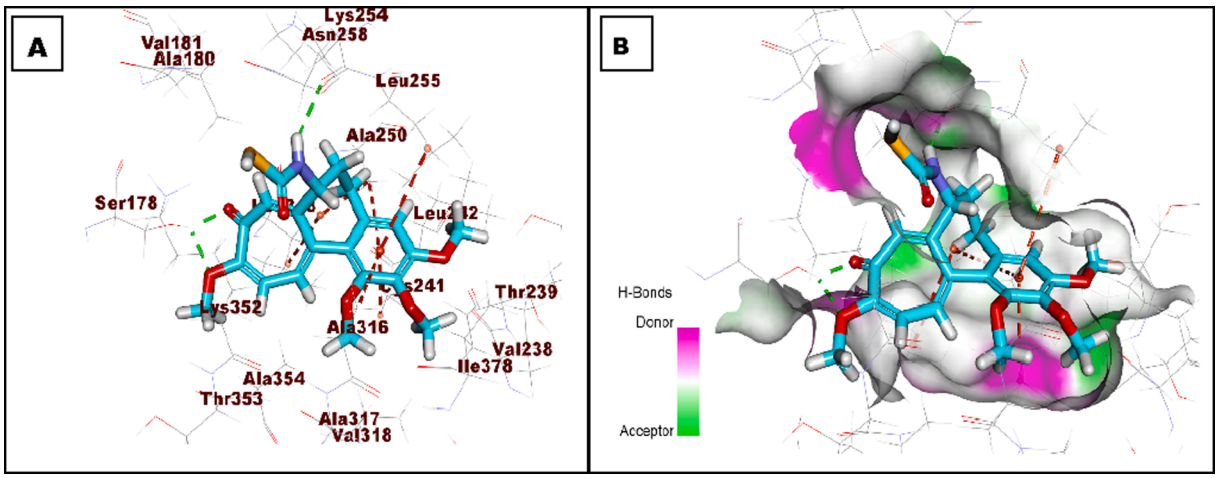

Fig. 8. A) 3D structure of co-crystallized ligand, DAMA-colchicine, docked into the colchicine binding site. **B)** Mapping surface showing DAMA-colchicine occupying the active pocket of colchicine binding site.

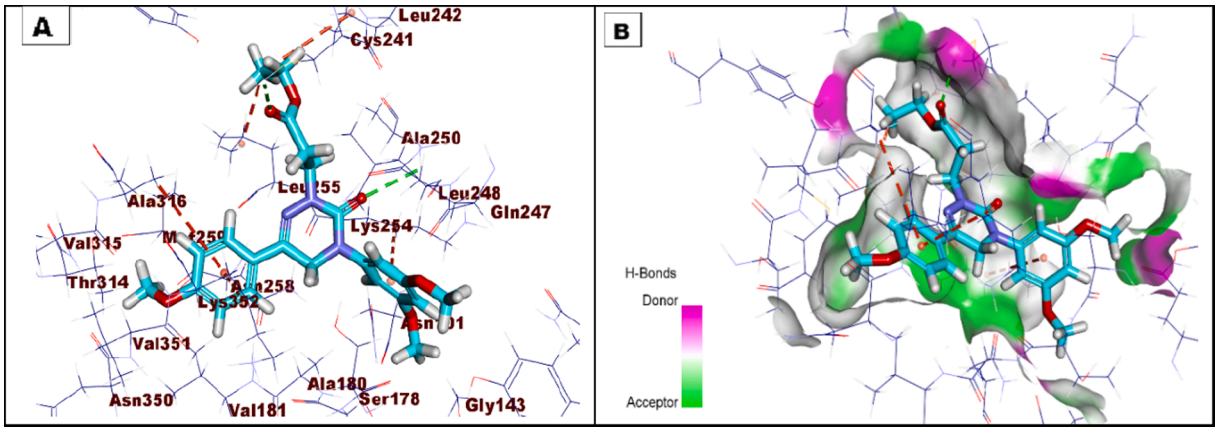

Fig. 9. A) 3D structure of compound **4i** docked into the colchicine binding site **B)** Mapping surface showing compound **4i** occupying the active pocket of colchicine binding site.

Table 7
Predicted ADMET for the designed compounds and reference drug.

Comp.	BBB level [a]	Solubility level [b]	Absorption level [c]	CYP2D6 prediction [d]	PPB prediction [e]
4i	3	3	0	FALSE	TRUE
4j	3	3	0	FALSE	TRUE
5 g	3	3	0	FALSE	TRUE
5i	3	3	0	FALSE	TRUE
6i	4	3	0	FALSE	TRUE
Colchicine	3	3	0	FALSE	FALSE

[a] Blood brain barrier (BBB) level, 0 = very high, 1 = high, 2 = medium, 3 = low, 4 = very low.
[b] Solubility level, 1 = very low, 2 = low, 3 = good, 4 = optimal.
[c] Absorption level, 0 = good, 1 = moderate, 2 = poor, 3 = very poor.
[d] CYP2D6, cytochrome P2D6, TRUE = inhibitor, FALSE = non inhibitor.
[e] PBB, plasma protein binding, FALSE means less than 90%, TRUE means>90%

3. Conclusion

Clearly the present work highlights the usefulness of the 1,2,4-triazines ring as a scaffold for synthesis of new colchicine analogues. We have designed and synthesized thirty-five final 1,2,4-triazin-3(2*H*)-one derivatives with different linkers. The design of these agents was based on the essential pharmacophoric features of the reported tubulin inhibitors. The newly synthesized compounds were evaluated for their anti-proliferative activities against three human cancer cell lines (MCF-7, HepG-2, and HCT-116). Compounds **4i, 4j, 5i, and 6i** were more active than colchicine as cytotoxic agents and tubulin polymerization inhibitors. SAR revealed that 3,5-dimethoxyphenyl and 3,4,5-trimethoxyphenyl miety is more beneficial as a "A" ring, while 4-methoxyphenyl moiety was more effective than phenyl ring as a "C" ring. Also, substitutions at the NH group of "B" ring with two carbon bridge acid, ester or amide is highly favorable. In order to get an additional comprehension about the effect of the synthesized compounds on the inhibition of cancer cell growth, the effect of compounds **3e** and **5i** on cell cycle distribution and apoptosis induction was analyzed. The most active compounds upregulated the level of active caspase 3 and Bax by five to seven folds comparing to the control. To further understand and rationalize the promising inhibitory profile of the compounds, docking studies were performed against the crystal structure of tubulin (PDB ID: 1SA0), which suggested that most of the synthesized compounds have similar binding mode with the target crystal structure. In silico ADMET, physico-chemical properties and toxicity studies were carried out for the most active compounds. Most of them were predicted to have low toxicity and good drug likeness. Further structural optimization of the most active candidates may serve as useful lead compounds in search for powerful and selective antineoplastic agents.

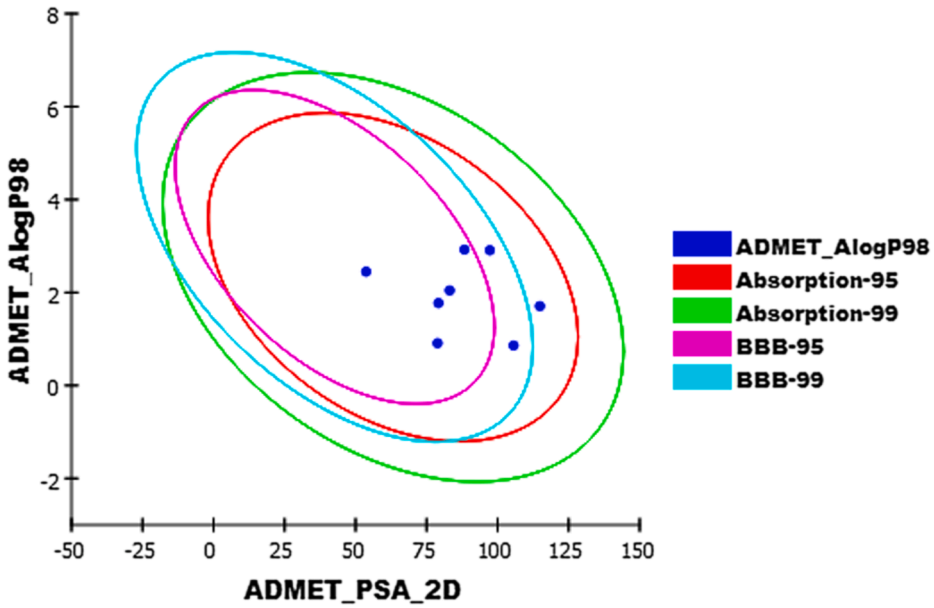

Fig. 10. The expected ADMET study of compounds **4i, 4j, 5 g, 5i,** and colchicine (These data were computationally generated using Discovery studio 4.0).

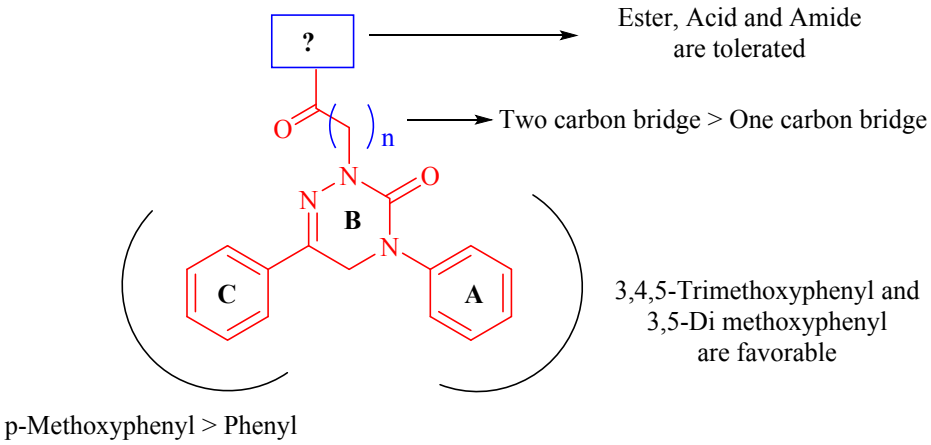

Fig. 11. Schematic diagram showing the SAR of the synthesized compounds.

4. Experimental

4.1. Chemistry

All commercially available materials were purchased from commercial sources and used without further purification·THF was passed through an activated alumina column embedded in a solvent purification system provided by LC Technology Solutions. All reactions were performed in a temperature-controlled oil/wax bath. Reactions were monitored by analytical thin layer chromatography (TLC), using aluminum-backed plates, cut to size. TLC visualization was achieved by UV and stain (such as KMnO4, ninhydrin and CAM). Flash column chromatography was carried out using 40–63 μm Silicycle silica gel. ^{1}H NMR and ^{13}C NMR spectra were recorded on Bruker AVANCE 300 MHz and 400 MHz spectrometers at ambient temperature. Spectral data is reported in ppm, coupling constants (*J*) in Hz. Infrared (IR) spectra were obtained as neat solids on Thermo Scientific Nicolet 6700 FTIR (ATR Diamond). High resolution mass spectroscopy (HRMS) was performed at the Ottawa-Carleton Mass Spectroscopy Centre on the Kratos Concept 11A mass spectrometer for Electron Impact (EI) and Waters Micromass Q-TOF I for electrospray ionization (ESI). All melting points were taken on a Gallenkamp melting point apparatus and are uncorrected. Nomenclature was determined using ChemBioDraw Ultra 14.0. The purity of the compounds, peak area percentage, was checked by HPLC analysis using Agilent 1200 Series instrument and Zorbax Rx-SIL column. The mobile phase was only prepared from HPLC grade solvents and all samples were filtered via a syringe filter prior to injection.

4.1.1. General procedure for synthesis of 1,2,4-triazin-3(2H)-ones (3a-e).

In a dry microwave vial equipped with a stir bar, α-amino ketone (1.05 equiv.) was added to phenyl carbazate (1.0 equiv.) and citric acid (1.0 equiv.). The vial was then sealed and purged with argon followed by the addition of purified THF (1.0 M). The resulting solution was left stirring at rt for 12–16 h. The reaction mixture was concentrated under reduced pressure, diluted with a saturated $NaHCO_3$ solution (20 mL) and extracted with EtOAc (3 × 10 mL). The organic layers were combined, dried with $NaSO_4$, filtered, and concentrated under reduced pressure. The crude products were purified by column chromatography or through recrystallization in MeOH.

4.1.1.1. 4,6-Diphenyl-4,5-dihydro-1,2,4-triazin-3(2H)-one 3a.. White solid (0.186 g, 74%). MP = 200–202 °C; IR (ATR diamond): 3216, 3097, 1662, 1625, 1593, 1195, 772 cm^{-1}; ^{1}H NMR (400 MHz, $CDCl_3$) δ (ppm): 8.09 (s, 1H), 7.68 (ddd, *J* = 4.4, 2.5, 1.4 Hz, 2H), 7.44 (t, *J* = 2.7 Hz, 2H),

7.42 (dd, J = 2.7, 1.6 Hz, 4H), 7.40 (d, J = 3.1 Hz, 1H), 7.31 – 7.26 (m, 1H), 4.74 (s, 2H); ^{13}C NMR (101 MHz, $CDCl_3$) δ (ppm): 151.5, 143.3, 140.4, 133.4, 130.0, 129.2, 128.8, 126.6, 125.3, 124.5, 47.7; HRMS (EI): Exact mass calcd for $C_{15}H_{13}N_3O$ $[M]^+$: 251.1053. Found: 251.1056; HPLC analysis showed purity > 99%.

4.1.1.2. 6-(4-Methoxyphenyl)-4-phenyl-4,5-dihydro-1,2,4-triazin-3(2H) -one 3b.. White solid (0.149 g, 53%); TLC Rf = 0.14 in 5% EtOAc/CH_2Cl_2; MP = 198–200 °C; IR (ATR diamond): 3191, 3110, 2922, 1692, 1451, 1190, 826 cm^{-1}; ^{1}H NMR (400 MHz, $CDCl_3$) δ (ppm): 7.90 (s, 1H), 7.65 – 7.59 (m, 2H), 7.47 – 7.38 (m, 4H), 7.32 – 7.26 (m, 1H), 6.95 – 6.90 (m, 2H), 4.70 (s, 2H), 3.84 (s, 3H); ^{13}C NMR (101 MHz, $CDCl_3$) δ (ppm): 161.0, 151.6, 143.2, 140.5, 129.1, 126.8, 126.5, 126.0, 124.5, 114.1, 55.4, 47.6; HRMS (EI): Exact mass calcd for $C_{16}H_{15}N_3O_2$ $[M]^+$: 281.1159. Found: 281.1165; HPLC analysis showed purity > 99%.

4.1.1.3. 4,6-Bis(4-methoxyphenyl)-4,5-dihydro-1,2,4-triazin-3(2H)-one 3c.. White solid (0.186 g, 74%); TLC Rf = 0.23 in 5% EtOAc/CH_2Cl_2; MP = 195–197 °C; IR (ATR diamond): 3221, 3104, 1672, 1512, 1199, 802 cm^{-1}; ^{1}H NMR (400 MHz, $CDCl_3$) δ (ppm): 8.53 (s, 1H), 7.60 – 7.56 (m, 2H), 7.31 – 7.27 (m, 2H), 6.93 – 6.87 (m, 4H), 4.61 (s, 2H), 3.80 (s, 3H), 3.79 (s, 3H); ^{13}C NMR (101 MHz, $CDCl_3$) δ (ppm): 160.9, 158.1, 152.1, 142.6, 133.5, 126.8, 126.3, 126.1, 114.5, 114.1, 55.5, 55.3, 48.2; HRMS (EI): Exact mass calcd for $C_{15}H_{13}N_3O$ $[M]^+$: 311.1264. Found: 311.1288; HPLC analysis showed purity > 99%.

4.1.1.4. 4-(3,5-Dimethoxyphenyl)-6-(4-methoxyphenyl)-4,5-dihydro-1,2,4-triazin-3(2H)-one 3d.. White solid (0.186 g, 74%); TLC Rf = 0.23 in 5% EtOAc/CH_2Cl_2; MP = 187–189 °C; IR (ATR diamond): 3100, 2360, 1667, 1629, 1418, 1149, 850 cm^{-1}; ^{1}H NMR (400 MHz, $CDCl_3$) δ (ppm): 8.08 (s, 1H), 7.61 – 7.57 (m, 2H), 6.92 – 6.88 (m, 2H), 6.54 (d, J = 2.2 Hz, 2H), 6.36 (t, J = 2.2 Hz, 1H), 4.63 (s, 2H), 3.82 (s, 3H), 3.78 (s, 6H); ^{13}C NMR (101 MHz, $CDCl_3$) δ (ppm): 161.1, 151.5, 143.2, 142.3, 126.8, 125.9, 114.1, 103.2, 98.7, 55.5, 55.4, 47.7; HRMS (EI): Exact mass calcd for $C_{15}H_{13}N_3O$ $[M]^+$: 341.1370. Found: 341.1403; HPLC analysis showed purity > 99%.

4.1.1.5. 6-(4-Methoxyphenyl)-4-(3,4,5-trimethoxyphenyl)-4,5-dihydro-1,2,4-triazin-3(2H)-one 3e.. White solid (0.186 g, 74%); TLC Rf = 0.23 in 5% EtOAc/CH_2Cl_2; MP = 203–205 °C; IR (ATR diamond): 3215, 3110, 2926, 1682, 1593, 1131, 822 cm^{-1}; ^{1}H NMR (400 MHz, $CDCl_3$) δ (ppm): (ppm): 8.45 – 8.40 (m, 1H), 7.58 (d, J = 8.8 Hz, 2H), 6.89 (d, J = 8.8 Hz, 2H), 6.58 (s, 2H), 4.62 (s, 2H), 3.83 (s, 6H), 3.82 (s, 3H), 3.80 (s, 3H); ^{13}C NMR (101 MHz, $CDCl_3$) δ 161.05, 153.56, 151.90, 142.85, 137.02, 136.38, 126.85, 126.00, 114.14, 103.20, 60.85, 56.28, 55.40, 48.43; HRMS (EI): Exact mass calcd for $C_{15}H_{13}N_3O$ $[M]^+$: 371.1509. Found: 371.1476; HPLC analysis showed purity > 99%.

4.1.2. General procedure for synthesis of compounds (4a-j).

In a dry microwave vial equipped with a stir bar, 5 mL of dry DMF was added to NaH (60% dispersion in mineral oil, 1.10 mmol). Compound **3a-e** (1.00 mmol) in 5 mL of DMF was slowly added to the slurry with stirring. The reaction mixture was stirred until H_2 evolution ceased (10 min). The vial was then sealed and purged with argon followed by slowly addition of ethyl bromoacetate (1.50 mmol) or ethyl 3-bromopropionate (1.50 mmol). The reaction mixture was stirred at rt (for ethyl bromoacetate) or reflux (for ethyl 3-bromopropionate), then allowed to cool to rt. The reaction was quenched with 15 mL of water, then diluted with EtOAc. The organic layer was washed several times with water and brine. The organic layer was dried over Na_2SO_4 and concentrated. The crude products were purified by column chromatography or through recrystallization.

4.1.2.1. Ethyl 2-(3-oxo-4,6-diphenyl-4,5-dihydro-1,2,4-triazin-2(3H)-yl) acetate 4a.. White solid (0.320 g, 95%); TLC Rf = 0.3 in 10% EtOAc/CH_2Cl_2; MP = 121–123 °C; IR (ATR diamond): 2559, 1742, 1657, 1514, 1151, 750 cm^{-1}; ^{1}H NMR (400 MHz, $CDCl_3$) δ (ppm): 7.67 – 7.62 (m, 2H), 7.39 – 7.35 (m, 7H), 7.25 – 7.19 (m, 1H), 4.74 (s, 2H), 4.61 (s, 2H), 4.23 (q, J = 7.1 Hz, 2H), 1.29 (t, J = 7.2 Hz, 3H); ^{13}C NMR (101 MHz, $CDCl_3$) δ (ppm): 169.3, 151.2, 142.9, 141.0, 133.4, 130.0, 129.0, 128.7, 126.3, 125.4, 124.6, 61.2, 51.8, 48.1, 14.3; HRMS (EI): Exact mass calcd for $C_{19}H_{19}N_3O_3$ [M]+: 337.1421. Found: 337.1411; HPLC analysis showed purity 97.4%.

4.1.2.2. Ethyl 2-(6-(4-methoxyphenyl)-3-oxo-4-phenyl-4,5-dihydro-1,2,4-triazin-2(3H)-yl)acetate 4b. Yellow viscous oil (0.349 g, 95%); TLC Rf = 0.30 in 10% EtOAc/CH_2Cl_2; IR (ATR diamond): 2980, 1750, 1669, 1514, 1173, 732 cm^{-1}; ^{1}H NMR (400 MHz, $CDCl_3$) δ (ppm): 7.60 – 7.56 (m, 2H), 7.35 (d, J = 5.0 Hz, 4H), 7.26 – 7.15 (m, 1H), 6.90 – 6.85 (m, 2H), 4.68 (s, 2H), 4.58 (s, 2H), 4.22 (q, J = 7.1 Hz, 2H), 3.78 (s, 3H), 1.27 (t, J = 7.1 Hz, 3H); ^{13}C NMR (101 MHz, $CDCl_3$) δ (ppm): 169.4, 161.1, 151.4, 142.9, 141.0, 129.0, 127.0, 126.2, 126.0, 124.5, 114.1, 61.2, 55.4, 51.8, 48.0, 14.3;

HRMS (EI): Exact mass calcd for $C_{20}H_{21}N_3O_4$ [M]+: 367.1527. Found: 367.1542; HPLC analysis showed purity 98.1%.

4.1.2.3. Ethyl 2-(4,6-bis(4-methoxyphenyl)-3-oxo-4,5-dihydro-1,2,4-triazin-2(3H)-yl)acetate 4c.. White solid (0.377 g, 95%); TLC Rf = 0.30 in 10% EtOAc/CH_2Cl_2; MP = 140–142 °C; IR (ATR diamond): 2033, 1744, 1658, 1510, 1154, 731 cm^{-1}; ^{1}H NMR (400 MHz, $CDCl_3$) δ (ppm): 7.58 – 7.54 (m, 2H), 7.27 – 7.23 (m, 2H), 6.86 (ddd, J = 8.9, 4.2, 2.2 Hz, 4H), 4.63 (dd, J = 3.6, 1.8 Hz, 2H), 4.55 (d, J = 1.5 Hz, 2H), 4.20 (qd, J = 7.1, 2.0 Hz, 2H), 3.77 (dd, J = 3.0, 1.5 Hz, 3H), 3.75 (dd, J = 3.1, 1.5 Hz, 3H), 1.26 (td, J = 7.1, 1.7 Hz, 3H); ^{13}C NMR (101 MHz, $CDCl_3$) δ (ppm): 169.4, 161.0, 157.9, 151.5, 142.5, 134.0, 126.9, 126.2, 126.0, 114.3, 61.1, 55.5, 55.4, 51.8, 48.7, 14.2; HRMS (EI): Exact mass calcd for $C_{21}H_{23}N_3O_5$ [M]+: 397.1632. Found: 397.1631; HPLC analysis showed purity 97.3%.

4.1.2.4. Ethyl 2-(4-(3,5-dimethoxyphenyl)-6-(4-methoxyphenyl)-3-oxo-4,5-dihydro-1,2,4-triazin-2(3H)-yl)acetate 4d. White solid (0.405 g, 95%); TLC Rf = 0.30 in 10% EtOAc/CH_2Cl_2; MP = 149–151 °C; IR (ATR diamond): 2044, 1750, 1667, 1516, 1146, 741 cm^{-1}; ^{1}H NMR (400 MHz, $CDCl_3$) δ (ppm): 7.59 – 7.55 (m, 2H), 6.89 – 6.85 (m, 2H), 6.52 (d, J = 2.2 Hz, 2H), 6.32 (t, J = 2.2 Hz, 1H), 4.65 (s, 2H), 4.57 (s, 2H), 4.21 (q, J = 7.1 Hz, 2H), 3.79 (s, 3H), 3.75 (s, 6H), 1.27 (t, J = 7.1 Hz, 3H); ^{13}C NMR (101 MHz, $CDCl_3$) δ (ppm): 169.4, 161.1, 160.9, 151.2, 142.9, 142.8, 127.0, 125.9, 114.0, 103.2, 98.6, 61.1, 55.4, 51.7, 48.1, 14.2; HRMS (EI): Exact mass calcd for $C_{22}H_{25}N_3O_6$ [M]+: 427.1738. Found: 427.1721; HPLC analysis showed purity 95.2%.

4.1.2.5. Ethyl 2-(6-(4-methoxyphenyl)-3-oxo-4-(3,4,5-trimethoxy-phenyl)-4,5-dihydro-1,2,4-triazin-2(3H)-yl)acetate 4e. White solid (0.434 g, 95%); TLC Rf = 0.30 in 10% EtOAc/CH_2Cl_2; MP = 137–139 °C; IR (ATR diamond): 2940, 1731, 1666, 1594, 1144, 736 cm^{-1}; ^{1}H NMR (400 MHz, $CDCl_3$) δ (ppm): 7.59 – 7.55 (m, 2H), 6.89 – 6.85 (m, 2H), 6.56 (s, 2H), 4.67 (s, 2H), 4.56 (s, 2H), 4.20 (q, J = 7.1 Hz, 2H), 3.81 (s, 6H), 3.79 (d, J = 2.4 Hz, 6H), 1.26 (t, J = 7.1 Hz, 3H); ^{13}C NMR (101 MHz, $CDCl_3$) δ (ppm): 169.4, 161.1, 153.4, 151.4, 142.7, 136.9, 127.0, 125.9, 114.0, 103.2, 61.2, 60.8, 56.3, 55.4, 51.7, 48.9, 14.2; HRMS (EI): Exact mass calcd for $C_{23}H_{27}N_3O_7$ [M]+: 457.1844. Found: 457.1828; HPLC analysis showed purity 96.3%.

4.1.2.6. Ethyl 3-(3-oxo-4,6-diphenyl-4,5-dihydro-1,2,4-triazin-2(3H)-yl) propanoate 4f.. White solid (0.263 g, 75%); TLC Rf = 0.30 in 10% EtOAc/CH_2Cl_2; MP = 145–147 °C;

IR (ATR diamond): 2189, 1731, 1649, 1495, 1199, 772 cm^{-1}; ^{1}H NMR (300 MHz, $CDCl_3$) δ (ppm): 7.66 – 7.62 (m, 2H), 7.39 – 7.32 (m, 7H), 7.23 – 7.17 (m, 1H), 4.63 (s, 2H), 4.19 (t, J = 7.4 Hz, 2H), 4.12 (t, J = 7.1 Hz, 2H), 2.80 (t, J = 7.1 Hz, 2H), 1.25 – 1.20 (m, 3H); ^{13}C NMR

(101 MHz, $CDCl_3$) δ (ppm): 171.9, 151.0, 142.6, 141.1, 133.5, 129.9, 129.0, 128.7, 126.2, 125.3, 124.5, 60.5, 47.5, 45.9, 33.6, 14.3; HRMS (EI): Exact mass calcd for $C_{20}H_{21}N_3O_3$ [M]+: 351.1577. Found: 351.1554; HPLC analysis showed purity 98.1%.

4.1.2.7. Ethyl 3-(6-(4-methoxyphenyl)-3-oxo-4-phenyl-4,5-dihydro-1,2,4-triazin-2(3H)-yl)propanoate 4 g. Yellow oil (0.247 g, 65%); TLC Rf = 0.30 in 10% EtOAc/CH_2Cl_2; IR (ATR diamond): 2997, 1727, 1666, 1572, 1173, 733 cm^{-1}; ^1H NMR (400 MHz, $CDCl_3$) δ (ppm): 7.61 – 7.58 (m, 2H), 7.37 – 7.34 (m, 4H), 7.23 – 7.19 (m, 1H), 6.90 – 6.87 (m, 2H), 4.63 (s, 2H), 4.19 – 4.16 (m, 2H), 4.14 – 4.11 (m, 2H), 3.80 (s, 3H), 2.79 (t, J = 7.2 Hz, 2H), 1.23 (t, J = 7.1 Hz, 3H); ^{13}C NMR (101 MHz, $CDCl_3$) δ (ppm): 171.9, 161.0, 151.2, 142.6, 141.2, 129.0, 126.9, 126.1, 124.5, 114.1, 60.5, 55.4, 47.5, 45.8, 33.6, 14.2; HRMS (ESI): Exact mass calcd for $C_{21}H_{23}N_3O_4Na$ [M + Na] $^+$: 404.1581. Found: 404.1586; HPLC analysis showed purity 96.4%.

4.1.2.8. Ethyl 3-(4,6-bis(4-methoxyphenyl)-3-oxo-4,5-dihydro-1,2,4-triazin-2(3H)-yl)propanoate 4 h. White solid (0.337 g, 82%); TLC Rf = 0.30 in 10% EtOAc/CH_2Cl_2; MP = 146–148 °C; IR (ATR diamond): 2033, 1730, 1660, 1572, 1173, 733 cm^{-1}; ^1H NMR (400 MHz, $CDCl_3$) δ (ppm): 7.54 – 7.50 (m, 2H), 7.18 (d, J = 8.9 Hz, 2H), 6.84 – 6.80 (m, 4H), 4.50 (s, 2H), 4.12 – 4.08 (m, 2H), 4.08 – 4.00 (m, 2H), 3.71 (s, 3H), 3.68 (s, 3H), 2.72 (t, J = 7.1 Hz, 2H), 1.17 (t, J = 7.1 Hz, 3H); ^{13}C NMR (101 MHz, $CDCl_3$) δ (ppm): 171.9, 160.9, 157.8, 151.3, 142.3, 134.2, 126.8, 126.1, 114.2, 114.0, 60.4, 55.4, 55.3, 48.1, 45.7, 33.6, 14.2; HRMS (ESI): Exact mass calcd for $C_{22}H_{25}N_3O_5Na$ [M + Na] $^+$: 434.1687. Found: 434.1692; HPLC analysis showed purity 97.3%.

4.1.2.9. Ethyl 3-(4-(3,5-dimethoxyphenyl)-6-(4-methoxyphenyl)-3-oxo-4,5-dihydro-1,2,4-triazin-2(3H)-yl)propanoate 4i.. White solid (0.234 g, 55%); TLC Rf = 0.30 in 10% EtOAc/CH_2Cl_2; MP = 130–132 °C; IR (ATR diamond): 2043, 1713, 1661, 1513, 1149, 797 cm^{-1}; ^1H NMR (400 MHz, $CDCl_3$) δ (ppm): 7.59 – 7.55 (m, 2H), 6.88 – 6.84 (m, 2H), 6.49 (d, J = 2.2 Hz, 2H), 6.30 (t, J = 2.2 Hz, 1H), 4.57 (s, 2H), 4.18 – 4.13 (m, 2H), 4.13 – 4.08 (m, 2H), 3.78 (s, 3H), 3.74 (s, 6H), 2.77 (t, J = 7.1 Hz, 2H), 1.21 (t, J = 7.1 Hz, 3H); ^{13}C NMR (101 MHz, $CDCl_3$) δ (ppm): 171.9, 161.0, 160.9, 151.0, 143.0, 142.7, 126.9, 126.0, 114.1, 103.1, 98.4, 60.4, 55.5, 55.4, 47.5, 45.7, 33.6, 14.2; HRMS (ESI): Exact mass calcd for $C_{23}H_{27}N_3O_6Na$ [M + Na] $^+$: 464.1792. Found:464.1796; HPLC analysis showed purity 95%.

4.1.2.10. Ethyl 3-(6-(4-methoxyphenyl)-3-oxo-4-(3,4,5-trimethoxyphenyl)-4,5-dihydro-1,2,4-triazin-2(3H)-yl)propanoate 4j.. White solid (0.259 g, 55%); TLC Rf = 0.30 in 10% EtOAc/CH_2Cl_2; MP = 128–130 °C; IR (ATR diamond): 2833, 1728, 1662, 1592, 1122, 737 cm^{-1}; ^1H NMR (400 MHz, $CDCl_3$) δ (ppm): 7.58 – 7.53 (m, 2H), 6.87 – 6.82 (m, 2H), 6.51 (s, 2H), 4.57 (s, 2H), 4.13 (d, J = 7.2 Hz, 2H), 4.10 – 4.06 (m, 2H), 3.79 (s, 6H), 3.77 (s, 3H), 3.76 (s, 3H), 2.74 (t, J = 7.1 Hz, 2H), 1.19 (t, J = 7.2 Hz, 3H); ^{13}C NMR (101 MHz, $CDCl_3$) δ (ppm): 171.9, 161.0, 153.4, 151.3, 142.4, 137.0, 136.6, 126.8, 126.0, 114.0, 103.0, 60.8, 60.4, 56.2, 55.4, 48.2, 45.7, 33.6, 14.2; HRMS (EI): Exact mass calcd for $C_{24}H_{29}N_3O_7$ [M]+: 471.2000. Found:471.2014; HPLC analysis showed purity 95%.

4.1.3. General procedure for synthesis of compounds (5a-5j).

In a dry microwave vial equipped with a stir bar, ester derivatives **4a-j** (1.0 equiv.) in sufficient amount of methanol, then a methanolic solution of 2 N NaOH was added slowly. The resulting solution was left stirring at reflux for 3–4 h. At this point, we formed the sodium salt, the reaction mixture was concentrated under reduced pressure. After that, the reaction was quenched with 1 N HCl and extracted with EtOAc (3 × 10 mL). The organic layers were combined, dried with Na_2SO_4, filtered, and concentrated under reduced pressure. The crude products were purified by recrystallization in MeOH.

4.1.3.1. 2-(3-Oxo-4,6-diphenyl-4,5-dihydro-1,2,4-triazin-2(3H)-yl)acetic acid 5a.. White solid (0.293 g, 95%); MP = 205–207 °C; IR (ATR diamond): 3057, 2176, 1728, 1658, 1500, 1144, 772 cm^{-1}; ^1H NMR (400 MHz, $CDCl_3$) δ (ppm): 11.10 (s, 1H), 7.67 – 7.62 (m, 2H), 7.38 (dd, J = 2.7, 6.2 Hz, 7H), 7.26 – 7.21 (m, 1H), 4.73 (s, 2H), 4.64 (s, 2H); ^{13}C NMR (101 MHz, $CDCl_3$) δ (ppm): 174.2, 151.5, 143.2, 140.7, 133.2, 130.1, 129.1, 128.7, 126.6, 125.5, 124.8, 51.6, 48.2; HRMS (EI): Exact mass calcd for $C_{17}H_{15}N_3O_3$[M]+: 309. 1108. Found: 309.1105; HPLC analysis showed purity > 99%.

4.1.3.2. 2-(6-(4-Methoxyphenyl)-3-oxo-4-phenyl-4,5-dihydro-1,2,4-triazin-2(3H)-yl)acetic acid 5b.. White solid (0.3222 g, 95%); MP = 150–152 °C; IR (ATR diamond): 3060, 2501, 1742, 1632, 1514, 1147, 764 cm^{-1}; ^1H NMR (300 MHz, $CDCl_3$) δ (ppm): 10.77 (s, 1H), 7.61 – 7.56 (m, 2H), 7.38 – 7.33 (m, 4H), 7.25 – 7.19 (m, 1H), 6.91 – 6.86 (m, 2H), 4.70 (s, 2H), 4.62 (s, 2H), 3.80 (s, 3H); ^{13}C NMR (101 MHz, $CDCl_3$) δ (ppm): 174.0, 161.1, 151.6, 143.1, 140.8, 129.0, 127.1, 126.5, 125.8, 124.7, 114.1, 65.9, 55.4, 51.6, 48.1, 15.2; HRMS (EI): Exact mass calcd for $C_{18}H_{17}N_3O_4$ [M]+: 339. 1214.Found: 339.1236; HPLC analysis showed purity > 99%.

4.1.3.3. 2-(4,6-Bis(4-methoxyphenyl)-3-oxo-4,5-dihydro-1,2,4-triazin-2(3H)-yl)acetic acid 5c.. White solid (0.350 g, 95%); MP = 195–197 °C; IR (ATR diamond): 3041, 2879, 1744, 1642, 1509, 1151, 733 cm^{-1}; ^1H NMR (400 MHz, DMSO) δ (ppm): 12.73 (s, 1H), 7.68 – 7.64 (m, 2H), 7.32 – 7.28 (m, 2H), 6.96 – 6.91 (m, 4H), 4.75 (s, 2H), 4.37 (s, 2H), 3.75 (s, 3H), 3.73 (s, 3H); ^{13}C NMR (101 MHz, DMSO) δ (ppm): 171.0, 161.0, 157.6, 151.2, 143.0, 134.5, 127.5, 126.7, 126.1, 114.4, 114.3, 55.8, 55.7, 51.8, 48.4; HRMS (EI): Exact mass calcd for $C_{19}H_{19}N_3O_5$ [M]+: 369.1319. Found:369.1339; HPLC analysis showed purity > 99%.

4.1.3.4. 2-(4-(3,5-Dimethoxyphenyl)-6-(4-methoxyphenyl)-3-oxo-4,5-dihydro-1,2,4-triazin-2(3H)-yl)acetic acid 5d.. White solid (0.379 g, 95%); MP = 170–172 °C; IR (ATR diamond): 3078, 1747, 1631, 1516, 1149, 897 cm^{-1}; ^1H NMR (400 MHz, DMSO) δ (ppm): 12.76 (s, 1H), 7.71 – 7.66 (m, 2H), 6.97 – 6.93 (m, 2H), 6.58 (d, J = 2.2 Hz, 2H), 6.37 (t, J = 2.2 Hz, 1H), 4.78 (s, 2H), 4.38 (s, 2H), 3.76 (s, 3H), 3.71 (s, 6H); ^{13}C NMR (101 MHz, DMSO) δ (ppm): 171.0, 161.1, 160.7, 150.9, 143.5, 143.2, 127.6, 126.0, 114.5, 103.7, 98.2, 55.8, 55.8, 51.8, 47.8; HRMS (EI): Exact mass calcd for $C_{20}H_{21}N_3O_6$ [M]+: 399.1425. Found: 399.1420; HPLC analysis showed purity > 99%.

4.1.3.5. 2-(6-(4-Methoxyphenyl)-3-oxo-4-(3,4,5-trimethoxyphenyl)-4,5-dihydro-1,2,4-triazin-2(3H)-yl)acetic acid 5e.. White solid (0.407 g, 95%); MP = 235–237 °C; IR (ATR diamond): 2942, 2521, 1735, 1622, 1515, 1205, 769 cm^{-1}; ^1H NMR (400 MHz, $CDCl_3$) δ (ppm): 9.32 (s, 1H), 7.55 (d, J = 8.6 Hz, 2H), 6.86 (d, J = 8.7 Hz, 2H), 6.56 (s, 2H), 4.65 (s, 2H), 4.58 (s, 2H), 3.80 (s, 9H), 3.78 (s, 3H); ^{13}C NMR (101 MHz, $CDCl_3$) δ (ppm): 173.5, 161.2, 153.4, 151.7, 143.0, 136.9, 136.6, 127.0, 125.7, 114.1, 103.3, 60.9, 56.3, 55.4, 51.5, 48.9; HRMS (EI):Exact mass calcd for $C_{21}H_{23}N_3O_7$ [M]+: 429.1531. Found: 429.1561; HPLC analysis showed purity > 99%.

4.1.3.6. 3-(3-Oxo-4,6-diphenyl-4,5-dihydro-1,2,4-triazin-2(3H)-yl) propanoic acid 5f.. White solid (0.306 g, 95%); MP = 135–137 °C; IR (ATR diamond): 3095, 2579, 1728, 1636, 1497, 1195, 752 cm^{-1}; ^1H NMR (400 MHz, $CDCl_3$) δ (ppm): 7.66 – 7.63 (m, 2H), 7.39 – 7.34 (m, 7H), 7.25 – 7.22 (m, 1H), 4.68 (s, 2H), 4.20 (t, J = 6.9 Hz, 2H), 2.84 (t, J = 7.0 Hz, 2H); ^{13}C NMR (101 MHz, $CDCl_3$) δ (ppm): 177.2, 151.3, 142.9, 141.0, 133.3, 130.0, 129.1, 128.7, 126.4, 125.4, 124.7, 47.7, 45.6, 33.4; HRMS (EI): Exact mass calcd for $C_{18}H_{17}N_3O_3$ [M]+: 323.1264. Found: 323.1295; HPLC analysis showed purity > 99%.

4.1.3.7. 3-(6-(4-Methoxyphenyl)-3-oxo-4-phenyl-4,5-dihydro-1,2,4-triazin-2(3H)-yl) propanoic acid 5 g.. White solid (0.320 g, 95%); MP =

150–152 °C; IR (ATR diamond): 2942, 1703, 1656, 1512, 1170, 732 cm^{-1}; ^1H NMR (400 MHz, $CDCl_3$) δ (ppm): 10.57 (s, 1H), 7.61 – 7.56 (m, 2H), 7.39 – 7.31 (m, 4H), 7.24 – 7.18 (m, 1H), 6.90 – 6.87 (m, 2H), 4.61 (s, 2H), 4.17 (t, *J* = 7.0 Hz, 2H), 3.78 (s, 3H), 2.81 (t, *J* = 7.0 Hz, 2H); ^{13}C NMR (101 MHz, $CDCl_3$) δ (ppm): 177.11, 161.06, 151.46, 142.92, 141.04, 129.01, 126.97, 126.32, 125.93, 124.68, 114.11, 55.39, 47.57, 45.51, 33.45; HRMS (EI):Exact mass calcd for $C_{19}H_{19}N_3O_4$ [M]+: 353.1370. Found: 353.1395; HPLC analysis showed purity > 99%.

4.1.3.8. 3-(4,6-Bis(4-methoxyphenyl)-3-oxo-4,5-dihydro-1,2,4-triazin-2 (3H)-yl) propanoic acid 5 h.. White solid (0.364 g, 95%); MP = 162–164 °C; IR (ATR diamond): 2942, 1703, 1656, 1512, 1170, 732 cm^{-1}; ^1H NMR (400 MHz, $CDCl_3$) δ (ppm): 10.61 (s, 1H), 7.59 – 7.54 (m, 2H), 7.25 – 7.21 (m, 2H), 6.90 – 6.86 (m, 4H), 4.59 (s, 2H), 4.15 (t, *J* = 6.9 Hz, 2H), 3.79 (s, 3H), 3.77 (s, 3H), 2.80 (t, *J* = 6.9 Hz, 2H); ^{13}C NMR (101 MHz, $CDCl_3$) δ (ppm): 177.1, 161.0, 158.0, 151.7, 142.6, 134.0, 126.9, 126.4, 126.0, 114.4, 114.1, 55.5, 55.4, 48.3, 45.5, 33.5; HRMS (ESI): Exact mass calcd for $C_{20}H_{21}N_3O_5Na$ [M + Na] $^+$: 406.1374. Found: 406.1379; HPLC analysis showed purity > 99%.

4.1.3.9. 3-(4-(3,5-Dimethoxyphenyl)-6-(4-methoxyphenyl)-3-oxo-4,5-dihydro-1,2,4-triazin-2(3H)-yl) propanoic acid 5i.. White solid (0.392 g, 95%); MP = 172–174 °C; IR (ATR diamond): 3094, 2193, 1662, 1571, 1513, 1174, 799 cm^{-1}; ^1H NMR (400 MHz, $CDCl_3$) δ (ppm): 7.58 (d, *J* = 8.4 Hz, 2H), 6.88 (d, *J* = 8.4 Hz, 2H), 6.50 (d, *J* = 2.2 Hz, 2H), 6.33 (d, *J* = 2.3 Hz, 1H), 4.59 (s, 2H), 4.16 (t, *J* = 6.9 Hz, 2H), 3.80 (s, 3H), 3.76 (s, 6H), 2.82 (t, *J* = 6.9 Hz, 2H); ^{13}C NMR (101 MHz, $CDCl_3$) δ (ppm): 177.1, 161.1, 160.9, 151.3, 143.1, 142.8, 126.9, 125.8, 114.1, 103.3, 98.6, 55.5, 55.4, 47.7, 45.4, 33.5; HRMS (EI):Exact mass calcd for $C_{21}H_{23}N_3O_6$ [M]+: 413.1581. Found: 413.1607; HPLC analysis showed purity > 99%.

4.1.3.10. 3-(6-(4-Methoxyphenyl)-3-oxo-4-(3,4,5-trimethoxyphenyl)-4,5-dihydro-1,2,4-triazin-2(3H)-yl)propanoic acid 5j.. White solid (0.421 g, 95%); MP = 220–222 °C; IR (ATR diamond): 2942, 2360, 1717, 1643, 1594, 1126, 736 cm^{-1}; ^1H NMR (400 MHz, $CDCl_3$) δ (ppm): 7.59 – 7.55 (m, 2H), 6.89 – 6.86 (m, 2H), 6.54 (s, 2H), 4.60 (s, 2H), 4.14 (t, *J* = 7.0 Hz, 2H), 3.82 (s, 6H), 3.80 (s, 3H), 3.79 (s, 3H), 2.79 (t, *J* = 7.0 Hz, 2H); ^{13}C NMR (101 MHz, $CDCl_3$) δ (ppm): 176.5, 161.1, 153.4, 151.5, 142.8, 136.8, 126.9, 125.9, 114.1, 103.2, 60.9, 56.3, 55.4, 50.5, 48.4, 45.5, 33.4; HRMS (EI):Exact mass calcd for $C_{22}H_{25}N_3O_7$ [M]+: 443.1687. Found: 443.1712; HPLC analysis showed purity > 99%.

4.1.4. General procedure for synthesis of compounds (6a-6j).

In a dry microwave vial equipped with a stir bar, 5 mL of dry DMF was added to NaH (60% dispersion in mineral oil, 1.10 mmol). Compound **3a-e** (1.00 mmol) in 5 mL of DMF was slowly added to the slurry with stirring. The reaction mixture was stirred until H_2 evolution ceased (10 min). The vial was then sealed and purged with argon followed by slowly addition of iodoacetamide (1.5 mmol) or 3-chloropropionamide (1.5 mmol). The reaction mixture was stirred at rt (for iodoacetamide) or reflux (for 3-chloropropionamide), then allowed to cool to rt. The reaction was quenched with 15 mL of water, then diluted with EtOAc. The organic layer was washed several times with water and brine. The organic layer was dried over Na_2SO_4 and concentrated. The crude products were purified by column chromatography or through recrystallization.

*4.1.4.1. **2-(3-Oxo-4,6-diphenyl-4,5-dihydro-1,2,4-triazin-2(3H)-yl) acetamide 6a.***. White solid (0.231 g, 75%); TLC Rf = 0.3 in 3% MeOH/CH_2Cl_2; MP = 191–193 °C; IR (ATR diamond): 3185, 2178, 1651, 1593, 1498, 1146, 754 cm^{-1}; ^1H NMR (400 MHz, $CDCl_3$) δ (ppm): 7.63 – 7.59 (m, 2H), 7.37 – 7.31 (m, 7H), 7.20 (tt, *J* = 2.1, 7.1 Hz, 1H), 6.52 (s, 1H), 6.10 (s, 1H), 4.68 (s, 2H), 4.48 (s, 2H); ^{13}C NMR (101 MHz, $CDCl_3$) δ (ppm): 171.7, 151.5, 143.7, 140.8, 133.1, 130.2, 129.1, 128.7, 126.6, 125.5, 124.7, 53.5, 48.1; HRMS (EI): Exact mass calcd for $C_{17}H_{16}N_4O_2$ [M]+: 308. 1268.Found: 308.1268; HPLC analysis showed purity 99%.

4.1.4.2. 2-(6-(4-Methoxyphenyl)-3-oxo-4-phenyl-4,5-dihydro-1,2,4-triazin-2(3H)-yl)acetamide 6b.. Yellow viscous oil (0.229 g, 68%); TLC Rf = 0.30 in 3% MeOH/CH_2Cl_2; MP = 193–195 °C; IR (ATR diamond): 3056, 2543, 1728, 1640, 1146, 754 cm^{-1}; ^1H NMR (400 MHz, $CDCl_3$) δ (ppm): 7.62 – 7.59 (m, 2H), 7.40 – 7.33 (m, 4H), 7.25 – 7.22 (m, 1H), 6.90 – 6.87 (m, 2H), 6.30 (s, 1H), 5.77 (s, 1H), 4.71 (s, 2H), 4.52 (s, 2H), 3.81 (s, 3H); ^{13}C NMR (101 MHz, $CDCl_3$) δ (ppm): 171.6, 161.3, 151.7, 143.8, 140.8, 129.1, 127.1, 126.6, 125.5, 124.7, 114.2, 55.4, 53.7, 48.0; HRMS (EI): Exact mass calcd for $C_{18}H_{18}N_4O_3$ [M]+: 338. 1373.Found: 338.1358; HPLC analysis showed purity 98.1%.

*4.1.4.3. **2-(4,6-Bis(4-methoxyphenyl)-3-oxo-4,5-dihydro-1,2,4-triazin-2(3H)-yl) acetamide 6c.***. White solid (0.294 g, 80%); TLC Rf = 0.30 in 5% MeOH/CH_2Cl_2; MP = 195–197 °C; IR (ATR diamond): 3168, 2030, 1652, 1509, 1175, 828 cm^{-1}; ^1H NMR (400 MHz, $CDCl_3$) δ (ppm): 7.59 – 7.54 (m, 2H), 7.25 – 7.21 (m, 2H), 6.89 – 6.85 (m, 4H), 6.44 (s, 1H), 5.92 (s, 1H), 4.64 (s, 2H), 4.47 (s, 2H), 3.79 (s, 3H), 3.75 (s, 3H); ^{13}C NMR (101 MHz, $CDCl_3$) δ (ppm): 171.9, 161.2, 158.1, 151.8, 143.4, 133.7, 127.0, 126.4, 125.6, 114.4, 114.1, 55.5, 55.4, 53.7, 48.7; HRMS (EI): Exact mass calcd for $C_{19}H_{20}N_4O_4$ [M]+: 368. 1479. Found: 368.1484; HPLC analysis showed purity > 99%.

*4.1.4.4. **2-(4-(3,5-Dimethoxyphenyl)-6-(4-methoxyphenyl)-3-oxo-4,5-dihydro-1,2,4-triazin-2(3H)-yl)acetamide 6d.***. White solid (0.274 g, 69%); TLC Rf = 0.30 in 5% MeOH/CH_2Cl_2; MP = 205–207 °C; IR (ATR diamond): 3459, 3301, 1678, 1639, 1414, 1147, 731 cm^{-1}; ^1H NMR (400 MHz, $CDCl_3$) δ (ppm): 7.61 – 7.58 (m, 2H), 6.90 – 6.87 (m, 2H), 6.50 (d, *J* = 2.2 Hz, 2H), 6.34 (t, *J* = 2.2 Hz, 1H), 6.29 (s, 1H), 5.71 (s, 1H), 4.66 (s, 2H), 4.51 (s, 2H), 3.81 (s, 3H), 3.76 (s, 6H); ^{13}C NMR (101 MHz, $CDCl_3$) δ (ppm): 171.5, 161.3, 161.0, 151.5, 143.9, 142.5, 127.1, 125.5, 114.1, 103.4, 98.8, 55.5, 55.4, 53.7, 48.1; HRMS (EI): Exact mass calcd for $C_{20}H_{22}N_4O_5$ [M]+: 398. 1585.Found: 398.1583; HPLC analysis showed purity > 99%.

*4.1.4.5. **2-(6-(4-Methoxyphenyl)-3-oxo-4-(3,4,5-trimethoxyphenyl)-4,5-dihydro-1,2,4-triazin-2(3H)-yl)acetamide 6e.***. White solid (0.308 g, 72%); TLC Rf = 0.30 in 3% MeOH/CH_2Cl_2; MP = 240–242 °C; IR (ATR diamond): 3381, 3209, 1686, 1640, 1510, 1123, 740 cm^{-1}; ^1H NMR (400 MHz, $CDCl_3$) δ (ppm): 7.62 – 7.56 (m, 2H), 6.91 – 6.86 (m, 2H), 6.56 (s, 2H), 6.26 (s, 1H), 5.77 (s, 1H), 4.68 (s, 2H), 4.51 (s, 2H), 3.83 (s, 6H), 3.81 (d, *J* = 1.1 Hz, 6H); ^{13}C NMR (101 MHz, $CDCl_3$) δ (ppm): 171.5, 161.3, 153.5, 151.7, 143.6, 137.1, 136.6, 127.0, 125.5, 114.2, 103.3, 60.9, 56.3, 55.4, 53.7, 48.9; HRMS (EI): Exact mass calcd for $C_{21}H_{24}N_4O_6$ [M]+: 428. 1690.Found: 428.1688; HPLC analysis showed purity 98.8%.

4.1.4.6. 3-(3-Oxo-4,6-diphenyl-4,5-dihydro-1,2,4-triazin-2(3H)-yl) propenamide 6f. White solid (0.229 g, 71%); TLC Rf = 0.30 in 3% MeOH/CH_2Cl_2; MP = 127–129 °C; IR (ATR diamond): 3179, 2922, 1720, 1647, 1496, 1195, 751 cm^{-1}; ^1H NMR (400 MHz, $CDCl_3$) δ (ppm): 7.68 – 7.63 (m, 2H), 7.39 (dtd, *J* = 2.0, 3.6, 7.2 Hz, 6H), 7.35 – 7.32 (m, 2H), 6.44 (s, 1H), 5.6 (s, 1H), 4.70 (s, 2H), 4.18 (t, *J* = 6.7 Hz, 2H), 2.75 (t, *J* = 6.7 Hz, 2H); ^{13}C NMR (101 MHz, $CDCl_3$) δ (ppm): 173.6, 151.5, 142.9, 140.9, 133.2, 130.1, 129.1, 128.8, 125.3, 124.7, 47.9, 46.3, 35.3, 29.7; HRMS (EI): Exact mass calcd for $C_{18}H_{18}N_4O_2$ [M]+: 322. 1424.Found: 322.1441; HPLC analysis showed purity 97.9%.

*4.1.4.7. **3-(6-(4-Methoxyphenyl)-3-oxo-4-phenyl-4,5-dihydro-1,2,4-triazin-2(3H)-yl)propenamide 6 g.***. Yellow crystal (0.354 g, 72%); TLC Rf = 0.30 in 3% MeOH/CH_2Cl_2; MP = 190–192 °C; IR (ATR diamond): 3367, 3182, 1698, 1652, 1449, 1001, 759 cm^{-1}; ^1H NMR (400 MHz, $CDCl_3$) δ (ppm): 7.61 – 7.57 (m, 2H), 7.40 – 7.30 (m, 5H), 6.90 – 6.87 (m,

2H), 6.53 (s, 1H), 5.64 (s, 1H), 4.65 (s, 2H), 4.15 (t, $J = 6.7$ Hz, 2H), 3.81 (s, 3H), 2.73 (t, $J = 6.7$ Hz, 2H); ^{13}C NMR (101 MHz, $CDCl_3$) δ (ppm): 173.7, 161.1, 151.6, 142.9, 141.0, 129.1, 126.9, 126.5, 125.8, 124.7, 114.1, 55.4, 47.8, 46.2, 35.3; HRMS (EI): Exact mass calcd for $C_{19}H_{20}N_4O_3$ [M]+: 352. 1530.Found: 352.1540; HPLC analysis showed purity > 99%.

4.1.4.8. ***3-(4,6-Bis(4-methoxyphenyl)-3-oxo-4,5-dihydro-1,2,4-triazin-2(3H)-yl) propenamide 6 h.***. White solid (0.268 g, 70%); TLC Rf = 0.30 in 10% EtOAc/CH_2Cl_2; MP = 140–142 °C; IR (ATR diamond): 3392, 2029, 1697, 1652, 1515, 1173, 734 cm^{-1}; ^{1}H NMR (400 MHz, $CDCl_3$) δ (ppm): 7.59 – 7.54 (m, 2H), 7.24 – 7.19 (m, 2H), 6.90 – 6.86 (m, 4H), 6.61 (s, 1H), 5.68 (s, 1H), 4.59 (s, 2H), 4.12 (t, $J = 6.7$ Hz, 2H), 3.79 (s, 3H), 3.76 (s, 3H), 2.71 (t, $J = 6.7$ Hz, 2H); ^{13}C NMR (101 MHz, $CDCl_3$) δ (ppm): 173.8, 161.1, 158.1, 151.8, 142.5, 133.9, 126.9, 126.4, 125.9, 114.4, 114.1, 55.5, 55.4, 48.5, 46.2, 35.3; HRMS (EI): Exact mass calcd for $C_{20}H_{22}N_4O_4$ [M]+: 382. 1636.Found: 382.1636; HPLC analysis showed purity > 99%.

4.1.4.9. ***3-(4-(3,5-Dimethoxyphenyl)-6-(4-methoxyphenyl)-3-oxo-4,5-dihydro-1,2,4-triazin-2(3H)-yl)propenamide 6i.***. White solid (0.297 g, 72%); TLC Rf = 0.30 in 5% MeOH/CH_2Cl_2; MP = 170–172 °C; IR (ATR diamond): 3421, 3303, 1651, 1605, 1513, 1170, 799 cm^{-1}; ^{1}H NMR (400 MHz, $CDCl_3$) δ (ppm): 7.61 – 7.57 (m, 2H), 6.91 – 6.87 (m, 2H), 6.50 (d, $J = 2.2$ Hz, 1H), 6.48 (d, $J = 2.2$ Hz, 2H), 6.34 (s, 1H), 5.52 (s, 1H), 4.61 (s, 2H), 4.16 (t, $J = 6.7$ Hz, 2H), 3.81 (s, 3H), 3.76 (s, 6H), 2.75 (t, $J = 6.6$ Hz, 2H); ^{13}C NMR (101 MHz, $CDCl_3$) δ (ppm): 173.6, 161.1, 161.0, 151.4, 143.0, 142.7, 126.9, 125.8, 114.1, 103.4, 98.6, 55.5, 55.4, 47.9, 46.1, 35.3; HRMS (EI): Exact mass calcd for $C_{21}H_{24}N_4O_5$ [M]+: 412. 1741.Found: 412.1761; HPLC analysis showed purity > 99%.

4.1.4.10. ***3-(6-(4-Methoxyphenyl)-3-oxo-4-(3,4,5-trimethoxyphenyl)-4,5-dihydro-1,2,4-triazin-2(3H)-yl)propenamide 6j.***. White solid (0.309 g, 70%); TLC Rf = 0.30 in 5% MeOH/CH_2Cl_2; MP = 225–227 °C; IR (ATR diamond): 3394, 2937, 1663, 1629, 1595, 1124, 733 cm^{-1}; ^{1}H NMR (400 MHz, $CDCl_3$) δ (ppm): 7.61 – 7.56 (m, 2H), 6.91 – 6.87 (m, 2H), 6.53 (s, 2H), 6.45 (s, 1H), 5.66 (s, 1H), 4.62 (s, 2H), 4.14 (t, $J = 6.7$ Hz, 2H), 3.82 (s, 6H), 3.80 (d, $J = 0.7$ Hz, 6H), 2.74 (t, $J = 6.7$ Hz, 2H); ^{13}C NMR (101 MHz, $CDCl_3$) δ (ppm): 173.6, 161.2, 153.5, 151.6, 142.7, 137.0, 136.8, 126.9, 125.8, 114.1, 103.2, 60.9, 56.3, 55.4, 48.6, 46.1, 35.3; HRMS (EI): Exact mass calcd for $C_{22}H_{26}N_4O_6$ [M]+: 442. 1847.Found: 442.1875; HPLC analysis showed purity 99%.

4.2. Biological evaluation

4.2.1. In vitro cytotoxic activity

Evaluation of cytotoxic activity of the synthesized compounds was carried out using MTT assay protocol [81,97,98] against a group of cancer cell lines namely; colorectal carcinoma (HCT-116), Hepatocellular carcinoma (HepG-2) and breast cancer (MCF-7) and colchicine was used as a standard drug. The cells were obtained from ATCC (American Type Culture Collection) via the Holding company for biological products and vaccines (VACSERA) (Cairo, Egypt). The anti-cancer activity was measured quantitatively as follows:

Into a medium of RPMI-1640 with 10% fetal bovine serum, the cell lines were cultured. Then, penicillin (100 units/ml) and streptomycin (100 μg/ml) were added at 37 °C in a 5% CO_2 incubator. Next, seeding the cell lines in a 96-well plate was achieved by a density of 1.0×10^4 cells / well at 37 °C for 48 h under 5% CO_2. After incubation period, the cell lines were treated with different concentration of the synthesized compounds and incubated for 24 h. After treatment by 24 h, 20 μl of MTT solution (5 mg/ml) was added and incubated for 4 h. Dimethyl sulfoxide (100 μl) was added into each well to dissolve the formed purple formazan. The colorimetric assay was measured and recorded at absorbance of 570 nm using a plate reader (EXL 800, USA). The relative cell viability in percentage was calculated as (A570 of treated samples/ A570 of untreated sample) X 100. Results for IC_{50}values of the active compounds were summarized in Table 1. The toxicities of the most promising compounds against normal human cells (WI-38) were assessed in the same procedure.

4.2.2. Tubulin polymerization assay

The effect of the synthesized compounds on tubulin polymerization was assessed turbidimetrically using a fluorescent plate reader method [99]. At first, ten of the synthesized compounds and reference drug (colchicine) were incubated in mixture of purified bovine tubulin (10 μM) and buffer system containing 20% glycerol and 1 mM ATP at 37 °C. Then, the mixture cooled to 0 °C. The IC_{50} value was defined as the compound concentration that inhibited the extent of tubulin assembly by 50%.

4.2.3. Cell cycle analysis

HepG-2 cells were seeded at density of 2×10^5 cells per well and incubated for 24 h in six-well plates. Fetal bovine serum (FBS, 10%) was added, after that cells were incubated at 37 °C and 5% CO_2. The medium was replaced with (DMSO 1% v/v) containing the tested compounds **3e (**67.7 μM) and **5i (**8.2 μM) for HepG-2. Then, the cells were incubated for 48 h, washed with cold phosphate buffered saline (PBS), fixed with 70% ethanol, rinsed with PBS then stained with the DNA fluorochrome PI, kept for 15 min at 37 °C. Then samples were analyzed with a FACS Caliber flow cytometer [88].

4.2.4. Annexin V-FITC apoptosis assay

The effect of compound **3e** and **5i** on apoptosis induction was analyzed using Annexin V-FITC/PI apoptosis detection kit. In this test, HepG-2 cells were stained with Annexin V fluorescein isothiocyanate (FITC) and counterstained with propidium iodide (PI). Then, HepG-2 cells in densities of 2×10^5 per well were incubated with compounds **3e (**67.7 μM) and **5i (**8.2 μM) for HepG-2 for 48 h. Next, the cells were trypsinized, washed with phosphate-buffered saline (PBS), and stained for 15 min at 37 °C in the dark. Finally, FACS Caliber flow cytometer was used in analysis process [91].

4.2.5. Caspase-3 determination

The percentage of caspase-3 activation was determined using the Caspase- Invitrogen Caspase-3 ELISA Kit (KHO1091) following the manufacturer's instructions [100,101].

4.2.6. Bax determination (real-time PCR).

The effect of compounds **4i, 4j, 5 g, 5i** and **6i** on BAX expressions was determined at concentrations of 14.4, 18.5, 23.2, 8.2, and 11.2 μM, respectively after 48 h of treatment on HepG-2 cells, using real-time PCR. The expression level of BAX was determined using a SYBR Green qRT-PCR kit (Bioneer, Daejeon, Korea) according to the manufacturer's protocol. PCR reactions were performed using specific primers for BAX. BAX forward primer: 5′-GCCCTTTTGCTTCAGGGTTT-3′; BAX Reverse primer: 5′ TCCAATGTCCAGCCCATGAT-3′. The reactions were carried out in triplicate using an Eco Real-Time PCR system (San Diego, CA, USA) [102].

4.3. In silico studies

4.3.1. Flexible alignment and docking

The crystal structure of tubulin heterodimers was downloaded from the Protein Data Bank, http://www.rcsb.org/pdb (PDB ID: 1SA0, resolution: 3.58 Å) using Discovery Studio 4.0 software. Water molecules were removed from downloaded protein. Crystallographic disorders and unfilled valence atoms were corrected using alternate conformations and valence monitor options. Protein was subjected to energy minimization by applying CHARMm force fields for charge, and MMFF94 force

field for partial charge. Inflexibility of structure was obtained by creating fixed atom constraint. The binding site of the protein was defined and prepared for docking. DAMA-colchicine, colchicine and the designed compounds 2D structures were sketched using ChemBioDraw Ultra 14.0 and saved in MDL-SD file format. Next, the SD file was opened, 3D structures were protonated, and energy was minimized by applying CHARMm force fields for charge andMMFF94 force field for partial charge and then prepared for docking by optimization of the parameters. Docking was accomplished using CDOCKER-CHARMm-based technique in the interface of Accelry's Discovery Studio 4.0. A maximum of 10 conformers was considered for each molecule in the docking analysis. After that the docking scores (CDOCKER interaction energy) of the best -fitted conformation of each of the docked molecules with the amino acids at the tubulin heterodimers binding pocket were recorded [103-105].

4.3.2. *In silico ADMET analysis*

ADMET descriptors (absorption, distribution, metabolism, excretion and toxicity) of the compounds were determined using Discovery studio 4.0. At first, the CHARMM force field was applied then the compounds were prepared and minimized according to the preparation of small molecule protocol. Then ADMET descriptors protocol was applied to carry out these studies [104,105].

4.3.3. *Toxicity studies*

The toxicity parameters of the most promising members **4i, 4j, 5 g, 5i** and **6i** were calculated using Discovery studio 4.0. colchicine was used as a reference drug. At first, the CHARMM force field was applied then the compounds were prepared and minimized according to the preparation of small molecule protocol. Then different parameters were calculated from toxicity prediction (extensible) protocol.

4.3.4. *Physico-chemical properties and Lipinski rule of five*

The physico-chemical properties of the selected compounds were calculated using Discovery studio 4.0. At first, the CHARMM force field was applied then the compounds were prepared and minimized according to the preparation of small molecule protocol. Then different parameters were calculated from calculate molecular properties from small molecule protocol [103].

Declaration of Competing Interest

The authors declare that they have no known competing financial interests or personal relationships that could have appeared to influence the work reported in this paper.

Acknowledgment

We thank the University of Ottawa and NSERC for generous financial support. M.A.D thanks the Egyptian Ministry of High Education and Al-Azhar University, Cairo, Egypt for supporting the scholarship. The authors extend their sincere appreciation to the Deanship of Scientific Research and the Research Center, College of Pharmacy, King Saud University for funding the biological testing and assay for the research project.

References

[1] E. Pasquier, M. Kavallaris, Microtubules: A dynamic target in cancer therapy, IUBMB Life 60 (3) (2008) 165–170.
[2] M.A. Jordan, Mechanism of action of antitumor drugs that interact with microtubules and tubulin, Curr Med Chem Anticancer Agents 2 (1) (2002) 1–17.
[3] Y.Y. Leung, L.L. Yao Hui, V.B. Kraus, Colchicine-Update on mechanisms of action and therapeutic uses, Seminars in arthritis and rheumatism 45 (3) (2015) 341–350.
[4] G.I. Varughese, A.I. Varghese, Colchicine in acute gouty arthritis: the optimum dose? Arthritis research & therapy 8 (5) (2006) 405.
[5] N. Dalbeth, T.J. Lauterio, H.R. Wolfe, Mechanism of action of colchicine in the treatment of gout, Clin Ther 36 (10) (2014) 1465–1479.
[6] Restrepo-Escobar, M., M.d.J. Carmona-Franceschi, and J.H. Donado Gómez, Colchicine treatment in adult patients with knee osteoarthritis: Systematic review of the literature. Revista Colombiana de Reumatología (English Edition), 2017. 24(2): p. 102-111.
[7] S.R. Shah, et al., Effects of colchicine on pericardial diseases: a review of the literature and current evidence, Journal of community hospital internal medicine perspectives 6 (3) (2016) 31957.
[8] G. Lazaros, et al., The Role of Colchicine in Pericardial Syndromes, Curr Pharm Des 24 (6) (2018) 702–709.
[9] M. Spartalis, et al., The Beneficial Therapy with Colchicine for Atherosclerosis via Anti-inflammation and Decrease in Hypertriglyceridemia, Cardiovasc Hematol Agents Med Chem 16 (2) (2018) 74–80.
[10] S.M. Nidorf, P.L. Thompson, Why Colchicine Should Be Considered for Secondary Prevention of Atherosclerosis: An Overview, Clin Ther 41 (1) (2019) 41–48.
[11] M. Niu, et al., The discovery of potential tubulin inhibitors: A combination of pharmacophore modeling, virtual screening, and molecular docking studies, Journal of the Taiwan Institute of Chemical Engineers 45 (5) (2014) 2111–2121.
[12] B. Wolach, et al., Colchicine analogues: effect on amyloidogenesis in a murine model and in vitro, on polymorphonuclear leukocytes, Eur J Clin Invest 22 (9) (1992) 630–634.
[13] K. Larocque, et al., Novel analogue of colchicine induces selective pro-death autophagy and necrosis in human cancer cells, PLoS One 9 (1) (2014), e87064.
[14] A. Brossi, et al., Colchicine and its analogues: Recent findings, Medicinal Research Reviews 8 (1) (1988) 77–94.
[15] I.A. Gracheva, et al., Colchicine Alkaloids and Synthetic Analogues: Current Progress and Perspectives, Journal of Medicinal Chemistry 63 (19) (2020) 10618–10651.
[16] X. Yang, et al., Discovery of novel CA-4 analogs as dual inhibitors of tubulin polymerization and PD-1/PD-L1 interaction for cancer treatment, European Journal of Medicinal Chemistry 213 (2021), 113058.
[17] E.C. McLoughlin, N.M. O'Boyle, Colchicine-Binding Site Inhibitors from Chemistry to Clinic, *A Review*. Pharmaceuticals (Basel) 13 (1) (2020).
[18] E.C. McLoughlin, N.M. O'Boyle, Colchicine-Binding Site Inhibitors from Chemistry to Clinic: A Review, Pharmaceuticals (Basel, Switzerland) 13 (1) (2020) 8.
[19] G.M. Tozer, et al., The biology of the combretastatins as tumour vascular targeting agents, International journal of experimental pathology 83 (1) (2002) 21–38.
[20] G.M. Tozer, et al., Mechanisms associated with tumor vascular shut-down induced by combretastatin A-4 phosphate: intravital microscopy and measurement of vascular permeability, Cancer Res 61 (17) (2001) 6413–6422.
[21] G.M. Tozer, C. Kanthou, B.C. Baguley, Disrupting tumour blood vessels, Nat Rev Cancer 5 (6) (2005) 423–435.
[22] G.Ş. Karatoprak, et al., Combretastatins: An Overview of Structure, Probable Mechanisms of Action and Potential Applications, Molecules (Basel, Switzerland) 25 (11) (2020) 2560.
[23] I.G. Kirwan, et al., Comparative Preclinical Pharmacokinetic and Metabolic Studies of the Combretastatin Prodrugs Combretastatin A4 Phosphate and A1 Phosphate, Clinical Cancer Research 10 (4) (2004) 1446–1453.
[24] S. Aprile, et al., In Vitro Metabolism Study of Combretastatin A-4 in Rat and Human Liver Microsomes, Drug Metabolism and Disposition 35 (12) (2007) 2252–2261.
[25] Y. Jin, et al., 3D-QSAR Study of Combretastatin A-4 Analogs Based on Molecular Docking, Molecules 16 (8) (2011) 6684–6700.
[26] G.G. Choudhury, et al., Interaction of colchicine analogues with purified tubulin, FEBS Lett 161 (1) (1983) 55–59.
[27] G. Wang, et al., Design, synthesis, and anticancer evaluation of benzophenone derivatives bearing naphthalene moiety as novel tubulin polymerization inhibitors, Bioorganic Chemistry 104 (2020), 104265.
[28] G. Li, et al., Design, synthesis, and bioevaluation of pyrazolo[1,5-a]pyrimidine derivatives as tubulin polymerization inhibitors targeting the colchicine binding site with potent anticancer activities, European Journal of Medicinal Chemistry 202 (2020), 112519.
[29] J. He, et al., Synthesis, Biological Evaluation, and Molecular Docking of Arylpyridines as Antiproliferative Agent Targeting Tubulin, ACS Medicinal Chemistry Letters 11 (8) (2020) 1611–1619.
[30] Q. Guo, et al., Ligand- and structural-based discovery of potential small molecules that target the colchicine site of tubulin for cancer treatment, European Journal of Medicinal Chemistry 196 (2020), 112328.
[31] Y.-Y. Shao, et al., Synthesis and biological evaluation of novel shikonin-benzo[b] furan derivatives as tubulin polymerization inhibitors targeting the colchicine binding site, European Journal of Medicinal Chemistry 190 (2020), 112105.
[32] N.G. Barnes, et al., A 2-step synthesis of Combretastatin A-4 and derivatives as potent tubulin assembly inhibitors, Bioorganic & Medicinal Chemistry 28 (19) (2020), 115684.
[33] T.M. Beale, et al., A-ring dihalogenation increases the cellular activity of combretastatin-templated tetrazoles, ACS Med Chem Lett 3 (3) (2012) 177–181.
[34] T. Doura, et al., Combretastatin A4-β-Galactosyl Conjugates for Ovarian Cancer Prodrug Monotherapy, ACS Med Chem Lett 8 (2) (2017) 211–214.
[35] J.A. Hadfield, et al., Synthesis and evaluation of double bond substituted combretastatins, Eur J Med Chem 40 (6) (2005) 529–541.
[36] D. Simoni, et al., Heterocyclic and phenyl double-bond-locked combretastatin analogues possessing potent apoptosis-inducing activity in HL60 and in MDR cell lines, J Med Chem 48 (3) (2005) 723–736.

[37] L. Lee, et al., 1,2,3,4-tetrahydro-2-thioxopyrimidine analogs of combretastatin-A4, Eur J Med Chem 43 (9) (2008) 2011–2015.
[38] B.R. Henke, et al., A new series of estrogen receptor modulators that display selectivity for estrogen receptor beta, J Med Chem 45 (25) (2002) 5492–5505.
[39] M. Mustafa, et al., Synthesis, antiproliferative, anti-tubulin activity, and docking study of new 1,2,4-triazoles as potential combretastatin analogues, Eur J Med Chem 141 (2017) 293–305.
[40] R. Fürst, et al., Synthesis and antitumor-evaluation of cyclopropyl-containing combretastatin analogs, Bioorganic & Medicinal Chemistry Letters 19 (24) (2009) 6948–6951.
[41] L. Wang, et al., Potent, orally active heterocycle-based combretastatin A-4 analogues: synthesis, structure-activity relationship, pharmacokinetics, and in vivo antitumor activity evaluation, J Med Chem 45 (8) (2002) 1697–1711.
[42] F. Yang, et al., Synthesis, and biological evaluation of 3,6-diaryl-[1,2,4]triazolo [4,3-a]pyridine analogues as new potent tubulin polymerization inhibitors, European Journal of Medicinal Chemistry 204 (2020), 112625.
[43] F. Yang, et al., Novel [1,2,4]triazolo[1,5-a]pyrimidine derivatives as potent antitubulin agents: Design, multicomponent synthesis and antiproliferative activities, Bioorganic Chemistry 92 (2019), 103260.
[44] Q. Li, et al., Synthesis and biological evaluation of benzofuran-based 3,4,5-trimethoxybenzamide derivatives as novel tubulin polymerization inhibitors, Bioorganic Chemistry 102 (2020), 104076.
[45] P. Diana, et al., Pyrrolo[2,1-c][1,2,4]triazines from 2-diazopyrroles: synthesis and antiproliferative activity, Eur J Med Chem 37 (3) (2002) 267–272.
[46] P. Barraja, et al., Synthesis and antiproliferative activity of [1,2,4]triazino [4,3-a] indoles, Anticancer Res 24 (6) (2004) 3775–3779.
[47] K. Sztanke, et al., Novel derivatives of methyl and ethyl 2-(4-oxo-8-aryl-2H-3,4,6,7-tetrahydroimidazo[2,1-c][1,2,4]triazin-3-yl)acetates from biologically active 1-aryl-2-hydrazinoimidazolines: synthesis, crystal structure and antiproliferative activity, Eur J Med Chem 41 (12) (2006) 1373–1384.
[48] T. El-Sayed Ali, Synthesis of some novel pyrazolo[3,4-b]pyridine and pyrazolo [3,4-d]pyrimidine derivatives bearing 5,6-diphenyl-1,2,4-triazine moiety as potential antimicrobial agents, Eur J Med Chem 44 (11) (2009) 4385–4392.
[49] O.Y. Voskoboynik, S.I. Kovalenko, S.V. Shishkina, Benzo[e][1,2,4]triazino[2,3-c] [1,2,3]triazin-2-ones electro-deficient heterocyclic compounds with promising anticancer activity, Heterocyclic Communications 22 (3) (2016) 137.
[50] S. Farhad, et al., Synthesis, Anti-proliferative Evaluation, and Molecular Docking Studies of 3-(alkylthio)-5,6-diaryl-1,2,4-triazines as Tubulin Polymerization Inhibitors, Letters in Drug Design & Discovery 16 (11) (2019) 1194–1201.
[51] W.M. Eldehna, et al., Novel 4/3-((4-oxo-5-(2-oxoindolin-3-ylidene) thiazolidin-2-ylidene) amino) benzenesulfonamides: Synthesis, carbonic anhydrase inhibitory activity, anticancer activity and molecular modelling studies, European journal of medicinal chemistry 139 (2017) 250–262.
[52] A.M. El-Naggar, et al., Design, eco-friendly synthesis, molecular modeling and anticancer evaluation of thiazol-5 (4 H)-ones as potential tubulin polymerization inhibitors targeting the colchicine binding site, RSC Advances 10 (5) (2020) 2791–2811.
[53] H.A. Mahdy, et al., Design, synthesis, molecular modeling, in vivo studies and anticancer evaluation of quinazolin-4 (3H)-one derivatives as potential VEGFR-2 inhibitors and apoptosis inducers, Bioorganic Chemistry 94 (2020), 103422.
[54] A.G.A. El-Helby, et al., Benzoxazole/benzothiazole-derived VEGFR-2 inhibitors: Design, synthesis, molecular docking, and anticancer evaluations, Archiv der Pharmazie 352 (12) (2019) 1900178.
[55] A.G.A. El-Helby, et al., Design, synthesis, molecular docking, and anticancer activity of benzoxazole derivatives as VEGFR-2 inhibitors, Archiv der Pharmazie 352 (10) (2019) 1900113.
[56] S.A. Elmetwally, et al., Design, synthesis and anticancer evaluation of thieno [2, 3-d] pyrimidine derivatives as dual EGFR/HER2 inhibitors and apoptosis inducers, Bioorganic chemistry 88 (2019), 102944.
[57] A.A. Gaber, et al., Design, synthesis and anticancer evaluation of 1H-pyrazolo [3, 4-d] pyrimidine derivatives as potent EGFRWT and EGFRT790M inhibitors and apoptosis inducers, Bioorganic chemistry 80 (2018) 375–395.
[58] K. El-Adl, et al., Design, synthesis, molecular docking and anticancer evaluations of 5-benzylidenethiazolidine-2, 4-dione derivatives targeting VEGFR-2 enzyme, Bioorganic Chemistry (2020), 104059.
[59] N.A. Alsaif, et al., New quinoxaline derivatives as VEGFR-2 inhibitors with anticancer and apoptotic activity: Design, molecular modeling, and synthesis, Bioorganic Chemistry 110 (2021), 104807.
[60] T.L. Nguyen, et al., A common pharmacophore for a diverse set of colchicine site inhibitors using a structure-based approach, Journal of medicinal chemistry 48 (19) (2005) 6107–6116.
[61] Y. Lu, et al., An overview of tubulin inhibitors that interact with the colchicine binding site, Pharmaceutical research 29 (11) (2012) 2943–2971.
[62] W. Li, et al., Tubulin inhibitors targeting the colchicine binding site: a perspective of privileged structures, Future Medicinal Chemistry 9 (15) (2017) 1765–1794.
[63] M.-M. Niu, et al., Tubulin inhibitors: pharmacophore modeling, virtual screening and molecular docking, Acta Pharmacologica Sinica 35 (7) (2014) 967–979.
[64] K. Ray, B. Bhattacharyya, B.B. Biswas, Role of B-ring of colchicine in its binding to tubulin, J Biol Chem 256 (12) (1981) 6241–6244.
[65] M. Cifuentes, et al., Synthesis and biological evaluation of B-ring modified colchicine and isocolchicine analogs, Bioorganic & Medicinal Chemistry Letters 16 (10) (2006) 2761–2764.
[66] L. Cosentino, et al., Synthesis and Biological Evaluation of Colchicine B-Ring Analogues Tethered with Halogenated Benzyl Moieties, Journal of Medicinal Chemistry 55 (24) (2012) 11062–11066.
[67] M.A. Dahab, J.S. Derasp, A.M. Beauchemin, Thieme Chemistry Journals Awardees – Where Are They Now?A Cascade Synthesis of 1,2,4-Triazin-3(2H)-ones Using Nitrogen-Substituted Isocyanates, Synlett 13 (04) (2017) 456–460.
[68] J.-F. Vincent-Rocan, et al., Cascade reactions of nitrogen-substituted isocyanates: a new tool in heterocyclic chemistry, Chemical Science 7 (1) (2016) 315–328.
[69] J.-F. Vincent-Rocan, J.S. Derasp, A.M. Beauchemin, Diversity-oriented heterocyclic synthesis using divergent reactivity of N-substituted iso(thio) cyanates, Chemical Communications 51 (91) (2015) 16405–16408.
[70] C. Clavette, et al., A Tunable Route for the Synthesis of Azomethine Imines and β-Aminocarbonyl Compounds from Alkenes, Journal of the American Chemical Society 134 (39) (2012) 16111–16114.
[71] R.A. Ivanovich, et al., One-Pot Synthesis of Aza-Diketopiperazines Enabled by Controlled Reactivity of N-Isocyanate Precursors, Org Lett 17 (19) (2015) 4898–4901.
[72] J.S. Derasp, J.F. Vincent-Rocan, A.M. Beauchemin, Divergent Reactivity of N-Isocyanates with Primary and Secondary Amines: Access to Pyridazinones and Triazinones, Org Lett 18 (4) (2016) 658–661.
[73] J. An, H. Alper, A.M. Beauchemin, Copper-Catalyzed Cascade Substitution/Cyclization of N-Isocyanates: A Synthesis of 1-Aminobenzimidazolones, Org Lett 18 (14) (2016) 3482–3485.
[74] A. Bongers, et al., Synthesis of Cyclic Azomethine Imines by Cycloaddition Reactions of N-Isocyanates and N-Isothiocyanates, Org Lett 18 (15) (2016) 3778–3781.
[75] J.-F. Vincent-Rocan, A.M. Beauchemin, N-Isocyanates, N-Isothiocyanates and Their Masked/Blocked Derivatives: Synthesis and Reactivity, Synthesis 48 (21) (2016) 3625–3645.
[76] A. Bongers, et al., Intermolecular Aminocarbonylation of Alkenes using Concerted Cycloadditions of Iminoisocyanates, The Journal of Organic Chemistry 82 (2) (2017) 1175–1194.
[77] E.B. Elkaeed, J. An, A.M. Beauchemin, Synthesis of Indazolones via Friedel-Crafts Cyclization of Blocked (Masked) N-Isocyanates, The Journal of Organic Chemistry 82 (18) (2017) 9890–9897.
[78] M.S. Mohamed, et al., Synthesis and kinetic testing of new inhibitors for a metallo-β-lactamase from Klebsiella pneumonia and Pseudomonas aeruginosa, European journal of medicinal chemistry 46 (12) (2011) 6075–6082.
[79] X. Li, et al., Synthesis of Multiple-Substituted Pyrroles via Gold(I)-Catalyzed Hydroamination/Cyclization Cascade, Org Lett 17 (12) (2015) 2984–2987.
[80] K. Garland, et al., A Practical Approach to Semicarbazone and Hydrazone Derivatives via Imino-isocyanates, Organic Letters 15 (16) (2013) 4074–4077.
[81] T. Mosmann, Rapid colorimetric assay for cellular growth and survival: Application to proliferation and cytotoxicity assays, Journal of Immunological Methods 65 (1) (1983) 55–63.
[82] M.I. Thabrew, R.D. Hughes, I.G. McFarlane, Screening of hepatoprotective plant components using a HepG2 cell cytotoxicity assay, J Pharm Pharmacol 49 (11) (1997) 1132–1135.
[83] A.A. Hyman, et al., Microtubule-motor activity of a yeast centromere-binding protein complex, Nature 359 (6395) (1992) 533–536.
[84] C.S. Sum, et al., Establishing a High-content Analysis Method for Tubulin Polymerization to Evaluate Both the Stabilizing and Destabilizing Activities of Compounds, Current chemical genomics and translational medicine 8 (Suppl 1) (2014) 16–26.
[85] Y.P. Quan, et al., Molecular modeling study, synthesis and biological evaluation of combretastatin A-4 analogues as anticancer agents and tubulin inhibitors, MedChemComm 9 (2) (2018) 316–327.
[86] J.-P. Liou, et al., Concise Synthesis and Structure−Activity Relationships of Combretastatin A-4 Analogues, 1-Aroylindoles and 3-Aroylindoles, as Novel Classes of Potent Antitubulin Agents, Journal of Medicinal Chemistry 47 (17) (2004) 4247–4257.
[87] H. Wang, et al., Erianin induces G2/M-phase arrest, apoptosis, and autophagy via the ROS/JNK signaling pathway in human osteosarcoma cells in vitro and in vivo, Cell Death & Disease 7 (6) (2016) e2247.
[88] J. Wang, M.J. Lenardo, Roles of caspases in apoptosis, development, and cytokine maturation revealed by homozygous gene deficiencies, J Cell Sci 113 (5) (2000) 753–757.
[89] J.M. Brown, B.G. Wouters, Apoptosis, p53, and tumor cell sensitivity to anticancer agents, Cancer Res 59 (7) (1999) 1391–1399.
[90] S. Fulda, Tumor resistance to apoptosis, International Journal of Cancer 124 (3) (2009) 511–515.
[91] K.K.-W. Lo, et al., Luminescent biological probes derived from ruthenium (II) estradiol polypyridine complexes, Inorganic Chemistry 47 (1) (2008) 200–208.
[92] A. Pérez-Garijo, When dying is not the end: Apoptotic caspases as drivers of proliferation, Seminars in Cell & Developmental Biology 82 (2018) 86–95.
[93] A.B. Parrish, C.D. Freel, S. Kornbluth, Cellular mechanisms controlling caspase activation and function, Cold Spring Harbor perspectives in biology 5 (6) (2013), a008672.
[94] B. Antonsson, Mitochondria and the Bcl-2 family proteins in apoptosis signaling pathways, Mol Cell Biochem 256–257 (1–2) (2004) 141–155.
[95] P.P. Roy, K. Roy, QSAR studies of CYP2D6 inhibitor aryloxypropanolamines using 2D and 3D descriptors, Chemical biology & drug design 73 (4) (2009) 442–455.
[96] T. Ghafourian, Z. Amin, QSAR models for the prediction of plasma protein binding, BioImpacts: BI 3 (1) (2013) 21.
[97] F. Denizot, R. Lang, Rapid colorimetric assay for cell growth and survival: modifications to the tetrazolium dye procedure giving improved sensitivity and reliability, Journal of immunological methods 89 (2) (1986) 271–277.

[98] Thabrew, M.I., R.D. HUGHES, and I.G. MCFARLANE, Screening of hepatoprotective plant components using a HepG2 cell cytotoxicity assay. Journal of pharmacy and pharmacology, 1997. 49(11): p. 1132-1135.
[99] G.M. Morris, et al., Automated docking using a Lamarckian genetic algorithm and an empirical binding free energy function, Journal of computational chemistry 19 (14) (1998) 1639–1662.
[100] Themo Fisher Scientific, Invitrogen Caspase 3 (Cleaved) Human ELISA Kit. Jan. 2020]; Available from: https://www.thermofisher.com/elisa/product/Caspase-3-Cleaved-Human-ELISA-Kit/KHO1091.
[101] Themo Fisher Scientific, Invitrogen Caspase 9 Human ELISA Kit ELISA Kit. Jan. 2020]; Available from: https://www.thermofisher.com/elisa/product/Caspase-9-Human-ELISA-Kit/BMS2025.
[102] T. Khanzadeh, et al., Investigation of BAX and BCL2 expression and apoptosis in a resveratrol-and prednisolone-treated human T-ALL cell line, *CCRF-CEM*. Blood research 53 (1) (2018) 53–60.
[103] K.M. El-Gamal, et al., Synthesis, docking, QSAR, ADMET and antimicrobial evaluation of new quinoline-3-carbonitrile derivatives as potential DNA-gyrase inhibitors, Journal of Molecular Structure 1166 (2018) 15–33.
[104] M.K. Ibrahim, et al., Design, synthesis, molecular modeling and anti-hyperglycemic evaluation of quinazolin-4 (3H)-one derivatives as potential PPARγ and SUR agonists, Bioorganic & medicinal chemistry 25 (17) (2017) 4723–4744.
[105] M.A. El-Zahabi, et al., Design, synthesis, molecular modeling and anti-hyperglycemic evaluation of phthalimide-sulfonylurea hybrids as PPARγ and SUR agonists, Bioorganic chemistry 91 (2019), 103115.